
Enhancing Federated Class-Incremental Learning via Spatial-Temporal Statistics Aggregation

Zenghao Guan^{1,2} Guojun Zhu¹ Yucan Zhou³ Wu Liu⁴ Weiping Wang² Jiebo Luo⁵ Xiaoyan Gu^{1,2}

Abstract

Federated Class-Incremental Learning (FCIL) enables Class-Incremental Learning (CIL) from distributed data. Existing FCIL methods typically integrate old knowledge preservation into local client training. However, these methods cannot avoid spatial-temporal client drift caused by data heterogeneity and often incur significant computational and communication overhead, limiting practical deployment. To address these challenges simultaneously, we propose a novel approach, **Spatial-Temporal Statistics Aggregation (STSA)**, which provides a unified framework to aggregate feature statistics both spatially (across clients) and temporally (across stages). The aggregated feature statistics are unaffected by data heterogeneity and can be used to update the classifier in closed form at each stage. Additionally, we introduce **STSA-E**, a communication-efficient variant with theoretical guarantee, achieving similar performance to STSA with much lower communication overhead. Extensive experiments on three widely used FCIL datasets, with varying degrees of data heterogeneity, show that our method outperforms state-of-the-art FCIL methods in terms of performance, flexibility, and both communication and computation efficiency. The code is available at <https://github.com/Yuqin-G/STSA>.

aggregates the model updates uploaded by clients rather than the private data. This mechanism addresses the data silos problem and provides privacy benefits for distributed learning (Kairouz et al., 2021).

Existing FL methods (McMahan et al., 2017; Dong et al., 2022) typically assume that data categories and domains remain static throughout the entire training and testing phases. However, this assumption fails to align with real-world environments, where data distributions are dynamic and continuously evolving (Yu et al., 2024; Li et al., 2024c; Yang et al., 2024; Li et al., 2024b). To tackle FL tasks in dynamic environments, recent research has incorporated Continual Learning (CL) techniques into the FL framework, giving rise to the approach known as Federated Continual Learning (FCL) (Dong et al., 2022; Ma et al., 2022; Yoon et al., 2021). In FCL, Federated Class-Incremental Learning (FCIL) (Zhang et al., 2023; Guo et al., 2024; Tran et al., 2024) has gained significant attention in recent years due to its wide applicability (Zhang et al., 2023; Kaissis et al., 2021). This setting allows new classes to be added flexibly at any time. In this paper, we focus on the global FCIL setting (Dong et al., 2022; 2023; Tran et al., 2024; Zhang et al., 2023; Guo et al., 2024), where a single global model is collaboratively trained across clients to learn new classes over time, aiming to enhance the generalization of the global model across all encountered classes.

In FCIL, we need to simultaneously address two core challenges: catastrophic forgetting and data heterogeneity. Existing FCIL methods typically follow the paradigm where the retention of old knowledge is integrated directly into local client training through techniques such as experience replay (Dong et al., 2022; 2023; Li et al., 2024a; Zhang et al., 2023; Qi et al.; Babakniya et al., 2023; Tran et al., 2024), weight regularization (Tan et al., 2024; Li et al.), and parameter-efficient fine-tuning (Ma'sum et al., 2024; Guo et al., 2024; Liu et al., 2023) (as shown in Figure 1). However, this paradigm still suffers from two critical drawbacks that limit its practical deployment. ① **Spatial-temporal client drift** caused by data heterogeneity. Specifically, each client has a distinct data distribution, leading to different balances in the optimization process between learning new tasks and preserving old knowledge. This disparity causes inconsis-

1. Introduction

Federated Learning (FL) (McMahan et al., 2017) is an emerging distributed machine learning framework that enables multiple parties to participate in collaborative learning (Li et al., 2025; Liu et al., 2024; 2025a;b; Li et al., 2026) under the coordination of a central server. The central server

¹University of Chinese Academy of Sciences ²State Key Laboratory of Cyberspace Security Defense, Institute of Information Engineering ³Tianjin University ⁴University of Science and Technology of China ⁵University of Rochester.

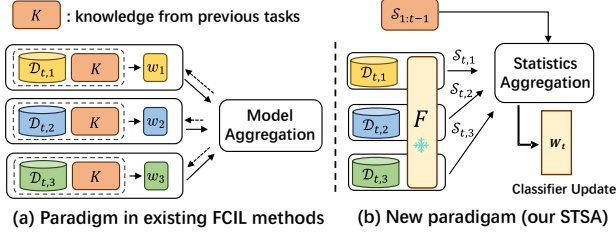


Figure 1. Paradigms of existing FCIL methods and ours. w and S denote the model weights and feature statistics, respectively.

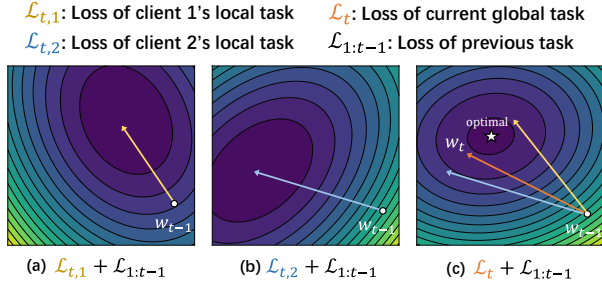


Figure 2. Illustration of spatial-temporal client drift through loss landscapes. W_t denotes the aggregated global model.

tent local updates, degrading the aggregated global model’s generalizability to both new and old tasks. As shown in Figure 2, we present the loss landscapes of the local and global models. The local model performs well on old tasks and current local tasks, but the global model shows a noticeable drift with the optimal model. ② **High communication and computation overhead.** Existing methods often necessitate iterative local updates and numerous communication rounds between clients and the server. This imposes significant computational burdens on client devices and leads to high communication overhead, posing practical limitations, especially for resource-constrained clients. These challenges motivated us to explore: *whether it is possible to break this paradigm and design a new method that effectively mitigates spatial-temporal client drift caused by data heterogeneity while maintaining low computational and communication overhead.*

In this paper, we propose a method named **Spatial-Temporal Statistics Aggregation (STSA)**. Instead of using aggregated local updates to update the global model, STSA aggregates feature statistics spatially (across clients) to learn new tasks and temporally (across stages) to retain old knowledge, using a fixed global feature extractor. Specifically, in the first stage of STSA, all clients engage in federated training to obtain a global model. The trained backbone is then fixed and distributed among all clients for feature statistics extraction at each subsequent stage. These statistics are first aggregated across clients and then across stages. Notably, the aggregated feature statistics are equivalent to those derived from all data samples across both dimensions due

to their linear characteristics, so **they are not affected by data heterogeneity**. Finally, these aggregated statistics are used to update the classifier in closed form at each stage. Since our method **requires no training** after the first stage and only needs one round of communication to upload feature statistics, it significantly improves computation and communication efficiency. Moreover, we propose a more communication-efficient variant, termed **STSA-E**, which enables the server to approximate global second-order feature statistics based on first-order statistics transmitted from clients. Theoretical analysis shows that STSA-E achieves similar statistical performance to STSA while considerably reducing communication overhead.

Extensive experiments on three widely used FCIL datasets demonstrate the superiority of our methods. In terms of performance, our STSA achieves over **10%** absolute improvements compared to the best-performing parameter-efficient fine-tuning baseline. Moreover, STSA achieves remarkable efficiency improvements, drastically reducing both communication and computation overhead. In particular, it delivers nearly **100×** faster computation compared to existing methods.

In summary, the main contributions of this paper are three-fold:

- We propose a novel FCIL method called STSA, which offers a unified way to aggregate feature statistics both spatially (across clients) and temporally (across stages). The aggregated feature statistics are immune to data heterogeneity and can be used to update the classifier in closed form at each stage.
- We propose STSA-E, a communication-efficient variant where the server approximates global second-order feature statistics using first-order statistics sent by clients. Theoretical and experimental results show that it achieves comparable performance to STSA while significantly reducing communication overhead.
- We conduct extensive experiments to validate our method. The results demonstrate significant improvements in performance, flexibility, and both communication and computational efficiency compared to state-of-the-art FCIL methods.

2. Method

2.1. Problem Definition

In FCIL, we have a set of T tasks $\mathcal{T} = \{\mathcal{T}_t\}_{t=1}^T$ shared among K clients, where the set of classes \mathcal{C}_t ($|\mathcal{C}_t| = c_t$) available at each time step t is disjoint. Each client k only have access to private dataset $\mathcal{D}_{t,k}$ with size $n_{t,k}$ at task \mathcal{T}_t . Here we denote $n_{t,k} \in \mathbb{R}^{c_t}$ as the label frequency.

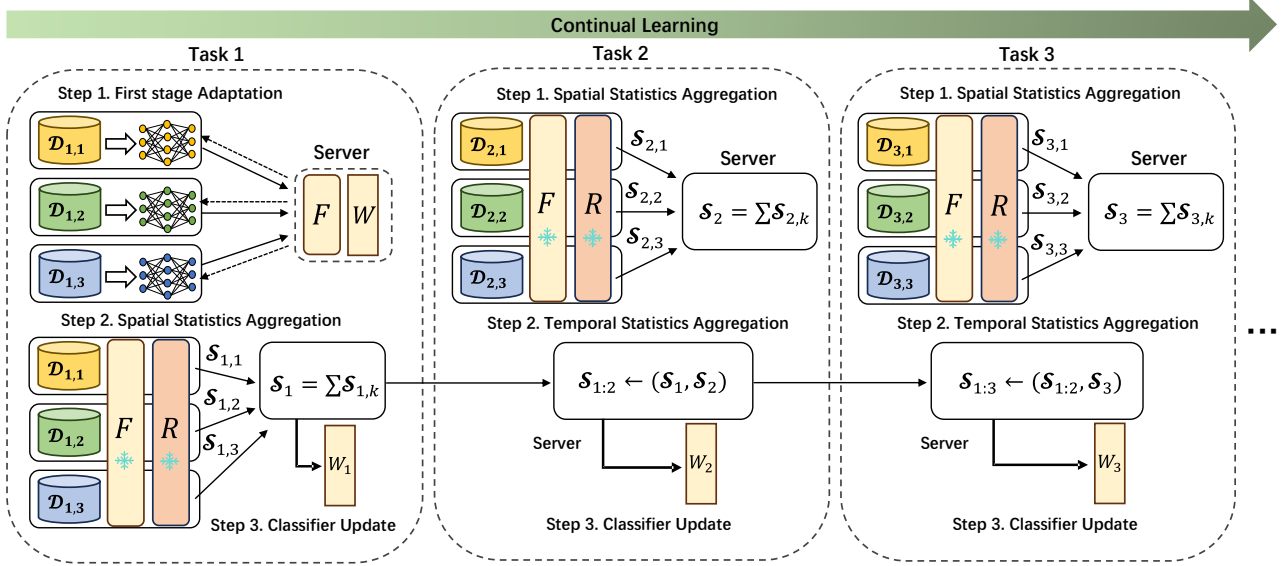


Figure 3. Framework of our algorithm. $\mathcal{D}_{i,j}$ denotes the local dataset of client j for task \mathcal{T}_i . F is the feature extractor trained in the first stage and is kept fixed afterward. R is the random mapping layer. In our STSA, Aggregated Spatial Statistics \mathcal{S}_t at stage t includes both \mathbf{G}_t and \mathbf{C}_t , whereas for STSA-E, it refers to \mathbf{C}_t .

During the training of task \mathcal{T}_t , each local client k trains its local model $\theta_{t,k}$ using its local data $\mathcal{D}_{t,k}$ and then uploads the updated model parameters to the server. The server aggregates the local models to obtain the global model θ_t and distribute it to all clients as the initialization for the next round of training. This process is repeated for multiple rounds, and the final global model θ_t can distinguish the samples belonged to the classes set $\bigcup_{i=1}^t \mathcal{C}_i$.

2.2. Spatial-Temporal Statistics Aggregation (STSA)

First Stage Adaptation. At task \mathcal{T}_1 , each client participates in federated training to obtain a global model θ_1 . Any federated learning algorithm can be used in this phase. After training, we freeze the feature extractor F from the global model θ_1 for further use.

Spatial Statistics Aggregation. For each task \mathcal{T}_t ($t > 0$), each client k uses this fixed feature extractor F to extract features from its local dataset. Given that the extracted features may lack sufficient expressiveness for clear class separation (Cover, 2006; McDonnell et al., 2024), we apply a nonlinear random mapping to project the extracted features into a higher-dimensional space (from d to M , $M > d$):

$$\mathbf{X}_{t,k} = [\Phi(x_1), \Phi(x_2), \dots, \Phi(x_{n_{t,k}})]^\top, \quad (1)$$

where $\{(x_i, y_i)\}_{i=1}^{n_{t,k}} = \mathcal{D}_{t,k}$, $\Phi = R \circ F$ represents the composition of the feature extractor F and the random mapping layer R , and $\mathbf{X}_{t,k} \in \mathbb{R}^{n_{t,k} \times M}$ denotes the concatenation of all feature vectors. Here, R consists of a random matrix followed by a ReLU function. This R is fixed after initialization and shared across all clients. To reduce storage overhead in the clients, the server can distribute a common seed to all clients. This allows clients to generate the same

random matrix locally using the seed. After obtaining high-dimensional features, clients can delete it and regenerate it when needed.

Subsequently, each client computes the local gram matrix $\mathbf{G}_{t,k} = \mathbf{X}_{t,k}^\top \mathbf{X}_{t,k} \in \mathbb{R}^{M \times M}$ and the feature-label correlation matrix $\mathbf{C}_{t,k} = \mathbf{X}_{t,k}^\top \mathbf{Y}_{t,k} \in \mathbb{R}^{M \times c_t}$. Here $\mathbf{Y}_{t,k}$ denotes the corresponding label matrix stacked by one-hot vectors. The Spatial Statistics $\mathcal{S}_{t,k} = \{\mathbf{G}_{t,k}, \mathbf{C}_{t,k}\}$ of each client k is then uploaded to the server and aggregated as follows:

$$\mathbf{G}_t = \sum_{k=1}^K \mathbf{G}_{t,k}, \quad \mathbf{C}_t = \sum_{k=1}^K \mathbf{C}_{t,k}. \quad (2)$$

Due to the linear additivity of these statistics, we have:

$$\begin{aligned} \mathbf{G}_{\text{centralized}} &= \sum_{(x,y) \in \mathcal{D}_t} \Phi(x)^\top \Phi(x) \\ &= \sum_{k=1}^K \sum_{(x,y) \in \mathcal{D}_{t,k}} \Phi(x)^\top \Phi(x) = \sum_{k=1}^K \mathbf{G}_{t,k} = \mathbf{G}_t. \\ \mathbf{C}_{\text{centralized}} &= \sum_{(x,y) \in \mathcal{D}_t} \Phi(x)^\top \text{OneHot}(y) \\ &= \sum_{k=1}^K \sum_{(x,y) \in \mathcal{D}_{t,k}} \Phi(x)^\top \text{OneHot}(y) = \sum_{k=1}^K \mathbf{C}_{t,k} = \mathbf{C}_t \end{aligned} \quad (3)$$

This demonstrates that the statistics derived from Spatial Statistics Aggregation are consistently equivalent to those from the centralized setting (with access to all data from all clients at stage t). Therefore, these statistics are invariant to varying levels of data heterogeneity.

Temporal Statistics Aggregation. The server then aggregates the Aggregated Spatial Statistics $\mathcal{S}_t = \{\mathbf{G}_t, \mathbf{C}_t\}$ with

Temporal Statistics $\mathcal{S}_{1:t-1} = \{\mathbf{G}_{1:t-1}, \mathbf{C}_{1:t-1}\}$, respectively:

$$\mathbf{G}_{1:t} = \mathbf{G}_{1:t-1} + \mathbf{G}_t, \quad \mathbf{C}_{1:t} = [\mathbf{C}_{1:t-1}, \mathbf{C}_t], \quad (4)$$

where $\mathbf{G}_{1:t-1} = \sum_{i=1}^{t-1} \mathbf{G}_i$ and $\mathbf{C}_{1:t-1} = [\mathbf{C}_1, \mathbf{C}_2, \dots, \mathbf{C}_{t-1}]$ are accumulated along $1 \sim (t-1)$ incremental stages. $\mathbf{G}_{1:t}$ and $\mathbf{C}_{1:t}$ are the latest Temporal Statistics need to store for further use. Given the linear additivity of these statistics, we have:

$$\begin{aligned} \mathbf{G}_{\text{joint}} &= \sum_{(x,y) \in \mathcal{D}_{1:t}} \Phi(x)^\top \Phi(x) = \sum_{i=1}^t \sum_{(x,y) \in \mathcal{D}_i} \Phi(x)^\top \Phi(x) = \mathbf{G}_{1:t} \\ \mathbf{C}_{\text{joint}} &= \sum_{(x,y) \in \mathcal{D}_{1:t}} \Phi(x)^\top \text{One-Hot}(y) \\ &= \sum_{i=1}^t \sum_{(x,y) \in \mathcal{D}_i} \Phi(x)^\top \text{One-Hot}(y) = \mathbf{C}_{1:t}. \end{aligned} \quad (5)$$

This indicates that the statistics derived through Temporal Statistics Aggregation are consistently equivalent to those obtained in the joint setting (with access to all data from task \mathcal{T}_1 to task \mathcal{T}_t).

Classifier Update. After the first stage adaptation, the backbone remains fixed, and only the classifier is updated. The objective of our STSA is to build a strong classifier capable of accurately distinguishing all previously encountered classes. We formulate the solving procedure of the classifier as a regularized least squares form (ridge regression):

$$\min_{\mathbf{W}} \|\mathbf{X}_{\text{joint}} \mathbf{W} - \mathbf{Y}_{\text{joint}}\|_{\text{F}}^2 + \gamma \|\mathbf{W}\|_{\text{F}}^2. \quad (6)$$

Here, $\mathbf{X}_{\text{joint}}$ represents the complete feature matrix, $\mathbf{Y}_{\text{joint}}$ represents the label matrix of all data samples from tasks \mathcal{T}_1 to \mathcal{T}_t , γ controls the strength of the regularization. The close-formed solution of Eq. 6 is:

$$\mathbf{W}^* = (\mathbf{G}_{\text{joint}} + \gamma \mathbf{I})^{-1} \mathbf{C}_{\text{joint}} \quad (7)$$

Based on Eq. 5, we have:

$$\begin{aligned} \mathbf{W}_t &= (\mathbf{G}_{1:t} + \gamma \mathbf{I})^{-1} \mathbf{C}_{1:t} \\ &= (\mathbf{G}_{\text{joint}} + \gamma \mathbf{I})^{-1} \mathbf{C}_{\text{joint}} = \mathbf{W}^*. \end{aligned} \quad (8)$$

Through our Spatial-Temporal Statistics Aggregation, we can obtain the feature statistics required for ridge regression on all data at any stage. Finally, the global model at the end of each stage t is $\theta_t = \{F, R, \mathbf{W}_t\}$.

Discussion. The rationale for STSA lies in the fact that the feature extractor is typically task-agnostic (Zhou et al., 2024a;b; Zhuang et al., 2022; McDonnell et al., 2024; Jiang et al., 2023; Zhou et al., 2024c). It learns to recognize "visual primitives", such as edges, textures. For example, an

extractor that learns "wheels" and "metal frames" from the "car" class can combine these "primitives" to build a strong representation for a newly introduced "bicycle" class. Consequently, the incremental learning simplifies from re-optimizing the entire feature space to learning a new decision boundary within an already expressive feature space. Built on this, our STSA extends online least squares (Farhang-Boroujeny, 2013; Camoriano et al., 2017; Zhuang et al., 2022; McDonnell et al., 2024; Guan et al.) to the FCIL scenario by providing a unified way to aggregate feature statistics across both temporal and spatial dimensions. In any scenario with restricted access to the complete dataset, the required statistics for ridge regression on the full dataset can be effectively obtained through our aggregation scheme.

2.3. A communication-efficient variant (STSA-E)

The communication overhead of uploading $\mathbf{G}_{t,k}$ ($M \times M$) increases significantly as M grows. To address this, we propose a communication-efficient variant of STSA, named STSA-E. It enables the server to approximate global second-order feature statistics \mathbf{G}_t using first-order statistics uploaded from clients.

Proposition 3.1 For each task \mathcal{T}_t ,

$$\begin{aligned} \hat{\mathbf{G}}_t &= \sum_{i=1}^{c_t} \left[\frac{n_t^{(i)} - 1}{K - 1} \sum_{k=1}^K \frac{(\mathbf{C}_{t,k}^{(i)}) (\mathbf{C}_{t,k}^{(i)})^\top}{n_t^{(i)}} \right. \\ &\quad \left. - \frac{n_t^{(i)} - K}{n_t^{(i)} (K - 1)} \left(\sum_{k=1}^K \mathbf{C}_{t,k}^{(i)} \right) \left(\sum_{k=1}^K \mathbf{C}_{t,k}^{(i)} \right)^\top \right] \quad (9) \end{aligned}$$

is an unbiased plug-in estimator of the global gram matrix \mathbf{G}_t when the global feature set $\Omega = \{(\Phi(x), y) \mid (x, y) \in \cup_{k=1}^K \mathcal{D}_{t,k}\}$ is i.i.d. Here, $\mathbf{C}_{t,k}^{(i)}$ represents the i -th column of $\mathbf{C}_{t,k}$, $n_t^{(i)}$ is the total number of samples from class i at stage t , and $n_{t,k}^{(i)}$ is the number of samples from class i for client k at stage t .

Remark 1. The i.i.d. assumption of the global feature set Ω in Proposition 3.1 is valid within the non-i.i.d. setting (data heterogeneity) in FCIL. We explain it in **Appendix B**.

Proposition 3.1 indicates that each client k only needs to transmit the correlation matrix $\mathbf{C}_{t,k}$ and the label frequency vector $\mathbf{n}_{t,k}$ ($\mathbf{n}_{t,k} \in \mathbb{R}^{c_t}$) for task t , significantly reducing communication overhead. The server leverages these uploaded statistics to compute the estimated gram matrix $\hat{\mathbf{G}}_t$ and performs temporal statistics aggregation (Eq. 4) to derive the accumulated global gram matrix $\hat{\mathbf{G}}_{1:t}$. Then $\mathbf{G}_{1:t}$ is used in Eq. 8 to update the classifier:

$$\mathbf{W}_t = (\hat{\mathbf{G}}_{1:t} + \gamma \mathbf{I})^{-1} \mathbf{C}_{1:t}. \quad (10)$$

Then we provide two key theoretical results to analyze the estimation error of STSA-E in comparison to STSA. The full descriptions and proofs can be found in **Appendix C**.

We consider a noisy linear regression model, where $n = \sum_{i=1}^t n_i$ and $n > M$. Specifically, we assume the existence of a ground-truth weight matrix $\mathbf{W}_t^0 \in \mathbb{R}^{M \times c_{\text{joint}}}$ and noise $\mathcal{E}_{\text{joint}} \in \mathbb{R}^{n \times c_{\text{joint}}}$ such that $\mathbf{Y}_{\text{joint}} = \mathbf{X}_{\text{joint}} \mathbf{W}_t^0 + \mathcal{E}_{\text{joint}}$, where $c_{\text{joint}} = \sum_i^t c_i$.

For each task \mathcal{T}_t , and for every $i \in \{1, \dots, c_t\}$, we make the following assumptions:

Assumption 1 (Data Structure). $\|\mathbf{X}_t\|_F \leq \sqrt{n_t} C_X$, $\text{tr}(\Sigma_t^{(i)}) \leq C_\Sigma$ and $\|\mu_t^{(i)}\|_2^2 \leq C_\mu$ for some constants $C_X, C_\Sigma, C_\mu > 0$, where $\mu_t^{(i)}$ and $\Sigma_t^{(i)}$ are the class-wise mean and covariance of the global feature set Ω at stage t .

Assumption 2 (Class Balance). There exists a constant $0 < C \ll c_t$ such that $c_t \sum_{i=1}^{c_t} n_t^{(i)2} \leq C n_t^2$.

Assumption 3 (Stability). $\|\mathbf{W}_t^0\|_F \leq \sqrt{M} r$ for some constant $r > 0$.

Assumption 4 (Noise). The i -th row of noise satisfies the following conditions: $\mathbb{E}(\mathcal{E}_{\text{joint},i}^\top) = \mathbf{0}$, $\mathbb{E}(\mathcal{E}_{\text{joint},i}^\top \mathcal{E}_{\text{joint},i}) = \sigma^2 \mathbf{I}_M$ and $\mathcal{E}_{\text{joint}}$ is independent of $\mathbf{X}_{\text{joint}}$.

These four assumptions are mild in statistical learning theory and aim to reflect practical conditions without overidealization. We provide a detailed explanation of their rationality in **Appendix C**.

Theorem 3.3 (STSA-E plug-in error). *Under Assumptions 1-2, with high probability, we have*

$$\frac{1}{n} \mathbb{E} \|\mathbf{X}_{\text{joint}} \mathbf{W}_t - \mathbf{X}_{\text{joint}} \mathbf{W}^*\|_F \leq O\left(\frac{\frac{K+1}{K-1} t}{n(\frac{\gamma^2}{n^2} + 1)}\right). \quad (11)$$

Remark 2. Theorem 3.3 shows that the plug-in error decreases as the average per-stage sample size $\frac{n}{t}$ increases.

Corollary 3.4 (Estimation error). *Under Assumptions 1-4, with high probability, we have*

$$\frac{1}{n} \mathbb{E} \|\mathbf{X}_{\text{joint}} \mathbf{W}_t - \mathbf{Y}_{\text{joint}}\|_F \leq O\left(\frac{\frac{K+1}{K-1} t}{n(\frac{\gamma^2}{n^2} + 1)}\right) + O\left(\frac{1}{\sqrt{n}}\right). \quad (12)$$

Remark 3. Corollary 3.4 reveals that our STSA-E achieves $O(tn^{-1})$ estimation efficiency, contrasting with the oracle estimator's $O(n^{-1/2})$ rate (Eq. 8) (Hsu et al., 2012). Thus, STSA-E maintains comparable statistical performance to the STSA with significantly reduced communication overhead, achieving a great performance-resource trade-off.

Dummy Clients. Since the number of clients, K , affects the quality of the estimated $\hat{\mathbf{G}}_t$, we introduce dummy clients to improve estimation when K is small (cross-silo setting).

Specifically, we divide each client's local dataset into multiple subsets, treating each subset as a separate dummy client. For instance, client k in task \mathcal{T}_t splits its dataset $\mathcal{D}_{t,k}$ into K_D subsets. Each dummy client k_j ($j = 1, 2, \dots, K_D$) holds a subset $\mathcal{D}_{t,k_j} \subset \mathcal{D}_{t,k}$ and uploads the corresponding spatial statistics \mathbf{C}_{t,k_j} and \mathbf{n}_{t,k_j} to the server. This effectively increases the number of clients from K to $K \times K_D$.

Discussion. Introducing dummy clients brings extra communication overhead for uploading first-order statistics (from $\mathbf{C}_{t,k}$ to $\{\mathbf{C}_{t,k_j}, \mathbf{n}_{t,k_j}\}_{j=1}^{K_D}$). However, this overhead is typically much smaller than the cost of uploading second-order statistics ($\mathbf{G}_{t,k}$) in STSA (see Section 3.4). It is worth noting that dummy clients are used to adapt STSA-E to the cross-silo setting, where the number of clients K is small. In the cross-device setting (K is large), they are not needed (see Section 3.3).

Figure 3 shows an overview of STSA and Algorithm 1 provides its entire procedure with pseudocode.

3. Experiments

3.1. Experimental Setting

Datasets and Models. We conduct experiments under two settings: training from scratch and training with a pre-trained model. For the scratch setting, we use ResNet18 (He et al., 2016) as the backbone on CIFAR100 (Krizhevsky et al., 2009) and Tiny-ImageNet (Le & Yang, 2015). For the pre-trained setting, we use ViT-B/16 (Dosovitskiy, 2020) (pre-trained on ImageNet-21K) as the backbone on CIFAR100 (Krizhevsky et al., 2009) and ImageNet-R (Hendrycks et al., 2021). By default, we divide dataset classes into 10 non-overlapping tasks ($T=10$) and distribute them among 5 clients ($K=5$) using a Dirichlet distribution with varying β .

Comparison Baselines. Following the benchmark in (Zhang et al., 2023; Tran et al., 2024), we compare our STSA and STSA-E with Fed-EWC (Kirkpatrick et al., 2017), Fed-LWF (Li & Hoiem, 2017), MFCL (Babakniya et al., 2023), and LANDER (Tran et al., 2024) under the training from scratch setting. We also evaluate our method against PEFT-based FCIL methods, including Fed-DualP (Wang et al., 2022), Fed-CODAP (Smith et al., 2023), Fed-CPrompt (Bagwe et al., 2023), and PiLoRA (Guo et al., 2024), using a pre-trained ViT-B/16. For our method, we integrate an adapter (Zhou et al., 2024a) with ViT to ensure performance after the first task is comparable to other PEFT-based methods.

Evaluation Metrics. The evaluation follows traditional CIL metrics (Smith et al., 2023; Wang et al., 2022; Zhou et al., 2024a), including: (1) average incremental accuracy A_{avg} , (2) final average accuracy A_T and (3) average forgetting F_T . Refer to **Appendix E.1** for further details on these metrics.

Experimental Details. For ResNet18, we set the batch size

Enhancing Federated Class-Incremental Learning via Spatial-Temporal Statistics Aggregation

Table 1. Experimental results for training from scratch (ResNet18) with varying levels of data heterogeneity. The best and second-best results are shown in **bold** and underlined, respectively.

Dataset	Data Partition Metrics	$\beta = 1$			$\beta = 0.5$			$\beta = 0.1$		
		$A_{\text{avg}} (\uparrow)$	$A_T (\uparrow)$	$F_T (\downarrow)$	$A_{\text{avg}} (\uparrow)$	$A_T (\uparrow)$	$F_T (\downarrow)$	$A_{\text{avg}} (\uparrow)$	$A_T (\uparrow)$	$F_T (\downarrow)$
CIFAR100	Joint (Upper-bound)	-	76.74	-	-	76.74	-	-	76.74	-
	Fed-EWC (Kirkpatrick et al., 2017)	29.23	11.76	73.52	27.16	11.56	70.53	21.21	9.13	60.79
	Fed-LWF (Li & Hoiem, 2017)	44.89	27.04	44.60	40.25	24.23	42.86	32.28	21.89	38.29
	MFCL (Babakniya et al., 2023)	43.48	26.46	31.28	44.00	27.17	27.27	34.48	21.96	22.77
	LANDER (Tran et al., 2024)	55.01	37.53	28.31	45.68	33.09	35.38	42.41	30.50	26.42
	STSA-E (Ours)	50.29	34.85	9.69	<u>49.16</u>	<u>34.57</u>	9.26	<u>44.86</u>	<u>30.74</u>	<u>9.92</u>
	STSA (Ours)	<u>50.71</u>	<u>35.14</u>	<u>9.81</u>	50.10	34.97	<u>9.57</u>	46.19	31.02	9.73
Tiny-ImageNet	Joint (Upper-bound)	-	49.44	-	-	49.44	-	-	49.44	-
	Fed-EWC (Kirkpatrick et al., 2017)	19.49	7.68	52.51	19.07	7.48	52.04	17.55	6.08	49.82
	Fed-LWF (Li & Hoiem, 2017)	29.11	17.02	27.64	26.91	15.47	28.06	26.54	15.16	25.22
	MFCL (Babakniya et al., 2023)	<u>32.58</u>	18.12	24.53	30.35	16.43	28.93	28.21	16.24	36.33
	LANDER (Tran et al., 2024)	34.53	18.21	38.04	30.75	16.59	26.77	28.49	16.29	33.76
	STSA-E (Ours)	30.86	<u>19.94</u>	<u>8.94</u>	30.91	20.02	<u>7.66</u>	<u>29.07</u>	<u>18.11</u>	<u>8.36</u>
	STSA (Ours)	31.14	20.03	8.26	<u>30.77</u>	<u>19.99</u>	6.56	29.10	18.18	7.50

Table 2. Experimental results for training from pre-trained model (ViT-B/16) with varying levels of data heterogeneity. The best and second-best results are shown in **bold** and underlined, respectively.

Dataset	Data Partition Metrics	$\beta = 1$			$\beta = 0.5$			$\beta = 0.1$		
		$A_{\text{avg}} (\uparrow)$	$A_T (\uparrow)$	$F_T (\downarrow)$	$A_{\text{avg}} (\uparrow)$	$A_T (\uparrow)$	$F_T (\downarrow)$	$A_{\text{avg}} (\uparrow)$	$A_T (\uparrow)$	$F_T (\downarrow)$
CIFAR100	Joint (Upper-bound)	-	92.45	-	-	92.45	-	-	92.45	-
	Fed-DualP (Wang et al., 2022)	83.02	75.07	4.78	78.12	65.77	3.97	69.11	56.31	3.31
	Fed-CODAP (Smith et al., 2023)	82.20	74.12	6.34	74.80	64.02	10.79	67.75	55.54	14.04
	Fed-CPrompt (Bagwe et al., 2023)	81.43	73.86	8.29	75.07	65.87	9.28	69.67	61.68	10.03
	PILoRA (Guo et al., 2024)	83.59	77.17	8.59	83.46	76.81	6.41	82.85	74.09	7.67
	STSA-E (Ours)	<u>93.71</u>	<u>89.42</u>	3.93	<u>93.35</u>	<u>89.37</u>	<u>4.05</u>	<u>93.14</u>	<u>88.65</u>	<u>4.06</u>
	STSA (Ours)	94.05	89.85	<u>4.12</u>	93.96	89.72	4.09	93.63	89.09	4.35
ImageNet-R	Joint (Upper-bound)	-	80.27	-	-	80.27	-	-	80.27	-
	Fed-DualP (Wang et al., 2022)	56.61	48.58	7.13	53.37	45.25	9.80	35.58	27.92	10.52
	Fed-CODAP (Smith et al., 2023)	55.10	51.13	6.42	48.49	43.00	6.06	23.22	15.15	8.29
	Fed-CPrompt (Bagwe et al., 2023)	51.09	47.28	9.49	45.42	39.12	9.27	23.67	16.87	9.52
	PILoRA (Guo et al., 2024)	55.47	51.92	6.69	53.43	50.18	7.09	51.85	47.85	7.19
	STSA-E (Ours)	<u>72.89</u>	<u>66.68</u>	<u>6.45</u>	<u>71.77</u>	<u>66.08</u>	<u>6.60</u>	71.67	<u>65.46</u>	6.37
	STSA (Ours)	74.02	67.25	6.84	73.59	66.67	7.14	73.65	66.78	<u>7.18</u>

to 128, local training epoch to 2, and communication rounds to 100. For pre-trained ViT-B/16, we use 2 local epochs with a batch size of 128, conducting 10 communication rounds on CIFAR100 and 20 communication rounds on ImageNet-R. The projection dimension of the adapter is set to 64. The dimension of the random feature M is set to 5000 for ResNet18 and 1250 for ViT-B/16. The number of dummy clients K_D is set to 50 for ResNet18, 10 for ViT-B/16. The ridge coefficient is set to $1e4$ for ResNet18 and $1e6$ for ViT-B/16. More details on configurations can be found in [Appendix E.2](#).

3.2. Main Results

Experiments for training from scratch. We present the results of experiments using ResNet18 in Table 1 and Figure 4. When data heterogeneity is low ($\beta = 1$), the DFKD method (LANDER, MFCL) performs well, and our method is slightly weaker than the best baseline, LANDER. However, as data heterogeneity increases, our method demon-

strates greater robustness. On CIFAR100, STSA shows significant performance improvements, particularly in average incremental accuracy. At $\beta = 0.5$, STSA-E outperforms LANDER by 3.48%, and STSA surpasses LANDER by 4.42%. Similarly, on Tiny-ImageNet, STSA shows substantial gains in final incremental accuracy. When $\beta = 0.5$, STSA-E outperforms LANDER by 3.43%, and STSA surpasses LANDER by 3.4%. Under extreme heterogeneity ($\beta = 0.1$), our method, like others, shows some performance drop due to the less effective feature extractor trained in the first stage. This drop can be mitigated by using better federated learning algorithms or a pre-trained model in the first stage.

Experiments for training from pre-trained model. The experimental results of training from pre-trained ViT-B/16 are shown in Table 2. We observe that STSA and STSA-E significantly outperforms the best FCIL baseline, achieving over **10%** improvements in both average incremental accuracy and final average accuracy across all cases. For CI-

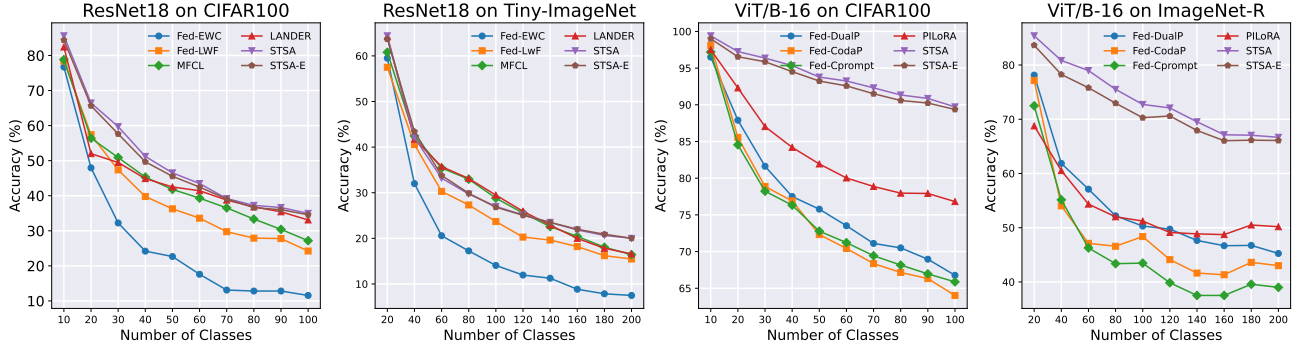


Figure 4. Performance curve of different datasets ($\beta = 0.5$) with different backbone.

FAR100, our method is just 3% lower than the upper bound. Furthermore, STSA and STSA-E exhibit strong robustness to data heterogeneity, maintaining nearly consistent performance regardless of the degree of heterogeneity. Moreover, we show the performance curve of different methods in Figure 4, which highlights the outstanding performance of our method throughout the entire incremental learning process. Compared to training from scratch, the pre-trained model’s generalizability enables it to learn a strong feature extractor in the first phase, which gives our method a significant performance advantage.

Comparison between STSA and STSA-E. STSA typically slightly outperforms STSA-E, though the reverse can occur, such as on Tiny-ImageNet ($\beta = 0.5$). This is due to estimation errors, which can be seen as random noise that sometimes enhances performance. As noted in Appendix F.2, adding random noise to feature statistics can sometimes improve performance. Similar findings have been reported in several FL studies (Zhang et al., 2024b;a). In summary, STSA-E delivers comparable performance to STSA while significantly reducing communication overhead (see Section 3.4). This makes STSA-E particularly well-suited for communication-constrained environments, such as mobile and IoT applications.

3.3. Ablation Study

We conduct the ablation study on the CIFAR100 with $\beta = 0.5$. Results for additional settings can be found in Appendix E.3.

Ablation on Dimension of Random Feature. Figure 5 shows the results with different values of M . Here, 512 is the dimension of raw feature in ResNet18, and 768 is the dimension of raw feature in ViT-B/16. We find that random mapping significantly improves the performance of STSA, confirming that random mapping enhances the linear separability of features. Additionally, setting M above 1250 is sufficient to achieve competitive results compared to other state-of-the-art baselines.

Ablation on Number of Clients. The number of clients varied as $K = \{5, 10, 25, 50\}$. For STSA-E, we set K_D to

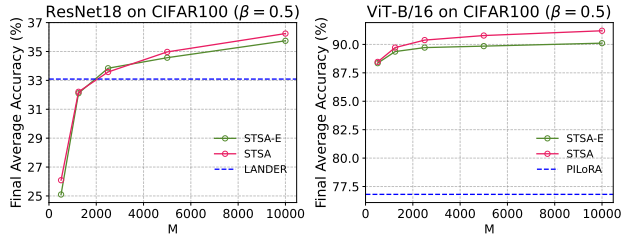


Figure 5. Final average accuracy A_T with different M . The top-performing baselines (LANDER and PILoRA) are also marked in the figure.

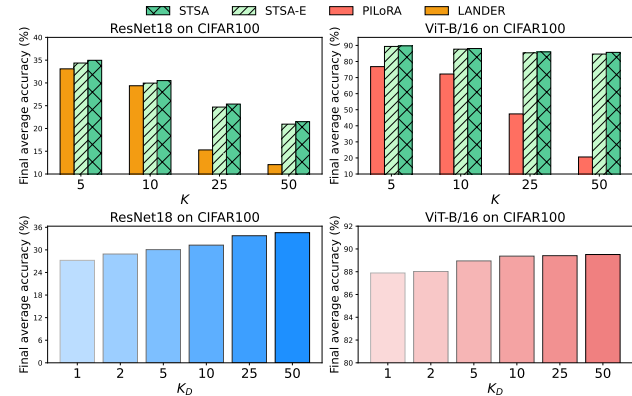


Figure 6. (Top) Final average accuracy with varying client number K . The top-performing baselines (LANDER and PILoRA) are also marked in the figure. (Bottom) Final average accuracy with varying dummy client number K_D .

$\{50, 25, 10, 5\}$ for ResNet18, totaling 250 clients ($K \times K_D$), and $\{10, 5, 2, 1\}$ for ViT-B/16, totaling 50 clients. Figure 6 (Top) demonstrates that our method outperforms other top-performing baselines as the number of clients increases. Notably, performance advantage becomes more evident with more clients, as only the first-stage adaptation is influenced by the number of clients, while the subsequent spatial-temporal statistics aggregation remains unaffected. Meanwhile, when the number of clients is large, there is no need to set dummy clients (ViT with $K = 50, K_D = 1$). Therefore, STSA-E is particularly well-suited for cross-device settings with many clients. We also assess the impact of varying the number of dummy clients K_D on the per-

formance of STSA-E. As shown in Figure 6 (Bottom), the performance of STSA-E improves with more dummy clients and gradually approaches that of STSA.

Ablation on First Stage adaptation Strategies. The subsequent statistics aggregation is independent of the first stage adaptation, so our STSA and STSA-E can combine with any PEFT methods for the first stage. Here, we combine two PEFT-based FCIL methods, PLoRA (LoRA) and FedCPrompt (prompt), with ours. Table 3 shows the results. We find that our STSA consistently achieves better performance against other baselines in all metrics. This demonstrates the high flexibility of our method.

PEFT	Metrics	$A_{\text{avg}}(\uparrow)$	$A_T(\uparrow)$	$F_T(\downarrow)$
LoRA	PiLoRA (Guo et al., 2024)	83.46	76.81	6.41
	STSA-E+PiLoRA	89.45	84.72	5.54
	STSA+PiLoRA	90.51	85.64	5.82
Prompt	Fed-CPrompt (Bagwe et al., 2023)	75.07	65.87	9.28
	STSA-E+Fed-CPrompt	90.07	85.67	5.26
	STSA+Fed-CPrompt	89.86	85.60	6.32
Adapter	STSA-E	<u>93.35</u>	<u>89.37</u>	<u>4.05</u>
	STSA	93.96	89.72	<u>4.09</u>

Table 3. Results of different first stage adaptation strategies. The dataset is CIFAR100 ($\beta = 0.5$).

3.4. Further Analysis

Large First Task Setting. The performance of our method relies on the feature extractor trained during the first incremental stage. A larger initial dataset improves the extractor’s quality. To examine this, we conduct experiments where the first task includes 50% of the total classes. Specifically, we partition the CIFAR100 dataset into 11 tasks: the base task (denoted as $t = 0$) contains 50 classes, while each subsequent task (for $t > 0$) consists of 5 classes. Table 4 presents the results. Our method consistently shows strong performance, outperforming top baselines by nearly 10% in all cases. This indicates that our method has the potential to achieve much better performance if the backbone trained in the first stage is strong enough.

Backbone	Metrics	$A_{\text{avg}}(\uparrow)$	$A_T(\uparrow)$	$F_T(\downarrow)$
ResNet18	LANDER (Tran et al., 2024)	59.69	46.19	13.61
	STSA-E (Ours)	<u>66.78</u>	<u>59.36</u>	<u>3.23</u>
	STSA (Ours)	67.08	59.44	2.69
ViT-B/16	PiLoRA (Guo et al., 2024)	86.24	81.44	4.21
	STSA-E (Ours)	<u>93.04</u>	<u>91.04</u>	2.14
	STSA (Ours)	93.70	91.57	<u>2.19</u>

Table 4. Comparison with top-performing baselines in Large First Task Setting.

Communication Overhead. After first stage adaptation, each client uploads only the Spatial Statistics, represented as $\{\mathbf{G}_{t,k}, \mathbf{C}_{t,k}\}$ with a size of $(M + c_t) \times M$ for STSA, or $\{\mathbf{C}_{t,k_j}, \mathbf{n}_{t,k_j}\}_{j=1}^{K_D}$ with a size of $(M + 1) \times c_t \times K_D$ for STSA-E at stage t . It is especially commendable that only one round of communication happens between the clients and the central server in the subsequent aggregation process,

Method	Communication Overhead \downarrow	Wallclock Time \downarrow
ResNet18 on CIFAR100 with 10 tasks, $M = 5000, K_D = 50$		
LANDER (Tran et al., 2024)	79047.9 MB	> 10 h
STSA-E (Ours)	95.4 MB	< 3 min
STSA (Ours)	955.6 MB	< 3 min
ViT-B/16 on CIFAR100 with 10 tasks, $M = 1250, K_D = 10$		
PiLoRA (Guo et al., 2024)	36.39 MB	> 20 h
STSA-E (Ours)	4.77 MB	< 10 min
STSA (Ours)	60.1 MB	< 10 min

Table 5. Cost comparison with top-performing baselines after the training in the first stage.

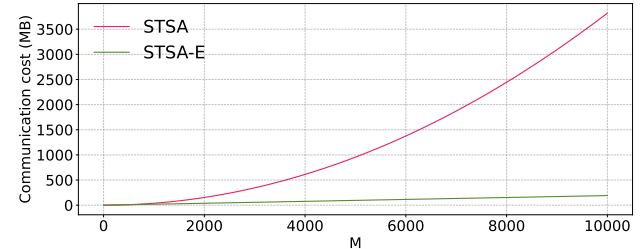


Figure 7. Communication overhead per client after the first stage of training, evaluated with varying M on CIFAR100 ($K_D = 50$).

which further reduces the potential risk for man-in-the-middle attacks (Guan et al., 2025; Dai et al., 2024). The left column of Table 5 presents the communication overhead of the entire learning process for each client. For fair comparison, we only evaluate communication overhead after the training in the first stage. Our method significantly reduces communication overhead compared to DFKD methods and achieves results comparable to PEFT methods. Figure 7 shows that our STSA-E significantly reduces communication overhead compared to STSA.

Computation Overhead. Our STSA does not involve the time-consuming backpropagation after the first stage adaptation, which provides a significant advantage in computational efficiency. We measure the total experimental time (including training and testing) after first stage adaptation using a single NVIDIA 3090 RTX GPU. As shown in the right columns in Table 5, our STSA is over 80 times faster than LANDER (Tran et al., 2024) and 120 times faster than PiLoRA (Guo et al., 2024).

Privacy of STSA. As same as PiLoRA (Guo et al., 2024), our method involves uploading feature statistics, which may raise privacy concerns. Specifically, STSA uploads $\mathbf{G}_{t,k}$ and $\mathbf{C}_{t,k}$, while STSA-E uploads $\mathbf{C}_{t,k}$ and $\mathbf{n}_{t,k}$ (assuming no dummy clients are used for simplicity). Feature statistics $\mathbf{G}_{t,k}$ and $\mathbf{C}_{t,k}$ are the aggregation of feature statistics from all local data samples. In real-world scenarios, each client k typically has many data samples across various classes, making it difficult to reconstruct specific samples from the uploaded feature statistics. To support this, we conduct feature inversion experiments (Ulyanov et al., 2018; Luo

et al., 2021) to validate this claim (**Appendix F.1**). Label frequency $n_{t,k}$ is widely used in various FL methods (Luo et al., 2021; Zhang et al., 2022; Gong et al., 2021; Zhu et al., 2021; Wang et al., 2024; Heinbaugh et al., 2023) and poses fewer privacy risks compared to data samples. Moreover, compatible privacy-preserving techniques, such as secure aggregation, can be integrated to further strengthen our method’s privacy protection, as the server requires only the aggregated Spatial Statistics rather than individual client values.

4. Related Work

Class-Incremental Learning. Continual learning (CL) enables a learning system to acquire knowledge from sequentially arriving tasks without catastrophic forgetting (Zhou et al., 2024d). In CL, Class-Incremental Learning (CIL) is the most popular setting due to its high relevance to real-world applications (Zhou et al., 2024d; Babakniya et al., 2023). In this setting, each new task introduces additional classes to the output space, progressively increasing the total number of classes. Existing CIL methods address catastrophic forgetting using various strategies, such as data replay (Aljundi et al., 2019; Shim et al., 2021), weight regularization (Ahn et al., 2019; Pan et al., 2020), knowledge distillation (Li & Hoiem, 2017; Simon et al., 2021), and network expansion (Wang et al., 2022; Smith et al., 2023; Zhou et al., 2024c). Although current CIL methods have made significant progress, they often struggle to perform well in the FCIL setting. This is due to the new challenges introduced by FL, such as data heterogeneity, communication constraints, and privacy concerns.

Federated Class-Incremental Learning. GLFC (Dong et al., 2022) is the first to introduce the FCIL setting and utilizes stored historical exemplars for local relation distillation. Various strategies are then proposed to make the best use of historical exemplars to mitigate catastrophic forgetting (Dong et al., 2023; Li et al., 2024a). However, storing data from previous tasks is prohibited due to strict privacy regulations and policies in many privacy-sensitive scenarios, e.g., hospitals and medical research institutions (Kaissis et al., 2021; Zhang et al., 2023; Tran et al., 2024). Therefore, the focus has shifted to more challenging exemplar-free scenarios. Existing state-of-the-art exemplar-free FCIL methods can be broadly classified into two categories: (1) Data-Free Knowledge Distillation (DFKD) approaches (Qi et al.; Babakniya et al., 2023; Zhang et al., 2023; Tran et al., 2024) and (2) Parameter-Efficient Fine-Tuning (PEFT) approaches (Ma’sum et al., 2024; Liu et al., 2023; Bagwe et al., 2023; Guo et al., 2024). DFKD-based FCIL methods train a generator to generate synthetic samples based on the predictions of the global model. These synthetic samples are stored for training subsequent tasks. However, storing and trans-

ferring large volumes of synthetic data between the server and clients would incur significant storage and communication costs. PEFT-based FCIL methods store knowledge from previous stages in prompt (Ma’sum et al., 2024; Liu et al., 2023; Bagwe et al., 2023) or LoRA (Guo et al., 2024) parameters and retain it using similarity matching or task arithmetic. However, these methods fail to fully exploit the generalization capabilities of pre-trained models (Zhou et al., 2024a) and remain vulnerable to spatial-temporal client drift, ultimately resulting in poor performance under high data heterogeneity. Besides, they suffer from computational inefficiency due to iterative backpropagation steps, placing a significant burden on client-side resources.

5. Conclusion and Future Work

We propose a novel FCIL method, STSA, which unifies feature statistic aggregation across spatial and temporal dimensions. The aggregated statistics are immune to data heterogeneity and enable closed-form classifier updates at each stage. We also introduce STSA-E, a variant that achieves similar performance with lower communication costs. Extensive experiments show that our method outperforms state-of-the-art baselines, offering greater flexibility while reducing communication and computation overhead. In the future, we plan to extend STSA to more FCL settings (e.g., asynchronous scenarios) and explore strategies for more efficient use of feature statistics.

Impact Statement

This paper aims to advance the field of Federated Class-Incremental Learning (FCIL). FCIL has the potential to enable privacy-preserving continual learning in decentralized environments. It allows edge devices (e.g., smartphones, wearables, and IoT sensors) to collaboratively build powerful models that can incrementally learn new tasks or classes over time without sharing raw data. This strengthens user privacy and ensures compliance with data protection regulations (e.g., GDPR). Our research enhances the effectiveness and efficiency of FCIL, enabling broader applications.

Acknowledgments

This work is supported by the Chinese Academy of Sciences under grant No. XDB0690302, the National Key Research and Development Program of China (NO. 2024YFE0203200), and the National Nature Science Foundation of China (NO. U24A20329).

References

Ahn, H., Cha, S., Lee, D., and Moon, T. Uncertainty-based continual learning with adaptive regularization. *Advances in neural information processing systems*, 32, 2019.

- Aljundi, R., Lin, M., Goujaud, B., and Bengio, Y. Gradient based sample selection for online continual learning. *Advances in neural information processing systems*, 32, 2019.
- Babakniya, S., Fabian, Z., He, C., Soltanolkotabi, M., and Avestimehr, S. A data-free approach to mitigate catastrophic forgetting in federated class incremental learning for vision tasks. In *Thirty-seventh Conference on Neural Information Processing Systems*, 2023.
- Bagwe, G., Yuan, X., Pan, M., and Zhang, L. Fed-cprompt: Contrastive prompt for rehearsal-free federated continual learning. *arXiv preprint arXiv:2307.04869*, 2023.
- Camoriano, R., Pasquale, G., Ciliberto, C., Natale, L., Rosasco, L., and Metta, G. Incremental robot learning of new objects with fixed update time. In *2017 IEEE International Conference on Robotics and Automation (ICRA)*, pp. 3207–3214. IEEE, 2017.
- Cover, T. M. Geometrical and statistical properties of systems of linear inequalities with applications in pattern recognition. *IEEE transactions on electronic computers*, (3):326–334, 2006.
- Dai, R., Zhang, Y., Li, A., Liu, T., Yang, X., and Han, B. Enhancing one-shot federated learning through data and ensemble co-boosting. In *The Twelfth International Conference on Learning Representations*, 2024.
- Ding, M., Ji, K., Wang, D., and Xu, J. Understanding forgetting in continual learning with linear regression. In *Proceedings of the 41st International Conference on Machine Learning*, pp. 10978–11001, 2024.
- Dong, J., Wang, L., Fang, Z., Sun, G., Xu, S., Wang, X., and Zhu, Q. Federated class-incremental learning. In *Proceedings of the IEEE/CVF conference on computer vision and pattern recognition*, pp. 10164–10173, 2022.
- Dong, J., Li, H., Cong, Y., Sun, G., Zhang, Y., and Van Gool, L. No one left behind: Real-world federated class-incremental learning. *IEEE Transactions on Pattern Analysis and Machine Intelligence*, 2023.
- Dosovitskiy, A. An image is worth 16x16 words: Transformers for image recognition at scale. *arXiv preprint arXiv:2010.11929*, 2020.
- Farhang-Boroujeny, B. *Adaptive filters: theory and applications*. John wiley & sons, 2013.
- Gong, X., Sharma, A., Karanam, S., Wu, Z., Chen, T., Doermann, D., and Innanje, A. Ensemble attention distillation for privacy-preserving federated learning. In *Proceedings of the IEEE/CVF International Conference on Computer Vision*, pp. 15076–15086, 2021.
- Guan, Z., Yucan, Z., Liu, W., and Gu, X. Statistics caching test-time adaptation for vision-language models. In *The Thirty-ninth Annual Conference on Neural Information Processing Systems*.
- Guan, Z., Zhou, Y., and Gu, X. Capture global feature statistics for one-shot federated learning. In *Proceedings of the AAAI Conference on Artificial Intelligence*, volume 39, pp. 16942–16950, 2025.
- Guo, H., Zhu, F., Liu, W., Zhang, X.-Y., and Liu, C.-L. Pilora: Prototype guided incremental lora for federated class-incremental learning. In *Proceedings of the European Conference on Computer Vision*, 2024.
- He, K., Zhang, X., Ren, S., and Sun, J. Deep residual learning for image recognition. In *Proceedings of the IEEE conference on computer vision and pattern recognition*, pp. 770–778, 2016.
- Heinbaugh, C. E., Luz-Ricca, E., and Shao, H. Data-free one-shot federated learning under very high statistical heterogeneity. In *The Eleventh International Conference on Learning Representations*, 2023.
- Hendrycks, D., Basart, S., Mu, N., Kadavath, S., Wang, F., Dorundo, E., Desai, R., Zhu, T., Parajuli, S., Guo, M., et al. The many faces of robustness: A critical analysis of out-of-distribution generalization. In *Proceedings of the IEEE/CVF international conference on computer vision*, pp. 8340–8349, 2021.
- Hsu, D., Kakade, S. M., and Zhang, T. Random design analysis of ridge regression. In *Conference on learning theory*, pp. 9–1. JMLR Workshop and Conference Proceedings, 2012.
- Jiang, M., Zeng, P., Wang, K., Liu, H., Chen, W., and Liu, H. Fecam: Frequency enhanced channel attention mechanism for time series forecasting. *Advanced Engineering Informatics*, 58:102158, 2023.
- Kairouz, P., McMahan, H. B., Avent, B., Bellet, A., Bennis, M., Bhagoji, A. N., Bonawitz, K., Charles, Z., Cormode, G., Cummings, R., et al. Advances and open problems in federated learning. *Foundations and Trends® in Machine Learning*, 14(1–2):1–210, 2021.
- Kaissis, G., Ziller, A., Passerat-Palmbach, J., Ryffel, T., Usynin, D., Trask, A., Lima Jr, I., Mancuso, J., Jungmann, F., Steinborn, M.-M., et al. End-to-end privacy preserving deep learning on multi-institutional medical imaging. *Nature Machine Intelligence*, 3(6):473–484, 2021.
- Kirkpatrick, J., Pascanu, R., Rabinowitz, N., Veness, J., Desjardins, G., Rusu, A. A., Milan, K., Quan, J., Ramalho, T., Grabska-Barwinska, A., et al. Overcoming catastrophic

- forgetting in neural networks. *Proceedings of the national academy of sciences*, 114(13):3521–3526, 2017.
- Krizhevsky, A., Hinton, G., et al. Learning multiple layers of features from tiny images. 2009.
- Le, Y. and Yang, X. Tiny imagenet visual recognition challenge. *CS 231N*, 7(7):3, 2015.
- Li, J., Liu, Y., Shang, Z., Gu, X., and Wang, W. DRGW: learning disentangled representations for robust graph watermarking. *arXiv:2601.13569*, 2026.
- Li, Q., Zhou, Y., Zhou, J., Yang, X., and Gu, X. Diverse and public features cooperation via gradient rectification for federated prompt learning. In *Proceedings of the 33rd ACM International Conference on Multimedia*, MM '25, 2025.
- Li, Y., Wang, Y., Wang, H., Qi, Y., Xiao, T., and Li, R. Fedssi: Rehearsal-free continual federated learning with synergistic synaptic intelligence. In *Forty-second International Conference on Machine Learning*.
- Li, Y., Li, Q., Wang, H., Li, R., Zhong, W., and Zhang, G. Towards efficient replay in federated incremental learning. In *Proceedings of the IEEE/CVF Conference on Computer Vision and Pattern Recognition*, pp. 12820–12829, 2024a.
- Li, Y., Wang, H., Xu, W., Xiao, T., Liu, H., Tu, M., Wang, Y., Yang, X., Zhang, R., Yu, S., et al. Unleashing the power of continual learning on non-centralized devices: A survey. *arXiv preprint arXiv:2412.13840*, 2024b.
- Li, Y., Xu, W., Wang, H., Qi, Y., Li, R., and Guo, S. Srdil: Synergistic replay for federated domain-incremental learning. *IEEE Transactions on Parallel and Distributed Systems*, 2024c.
- Li, Z. and Hoiem, D. Learning without forgetting. *IEEE transactions on pattern analysis and machine intelligence*, 40(12):2935–2947, 2017.
- Liu, J., Zhan, Y.-W., Zhang, C.-Y., Luo, X., Chen, Z.-D., Wei, Y., and Xu, X.-S. Federated class-incremental learning with prompting. *arXiv preprint arXiv:2310.08948*, 2023.
- Liu, Y., Liu, W., Gu, X., Rui, Y., He, X., and Zhang, Y. Lmagent: A large-scale multimodal agents society for multi-user simulation. *arXiv preprint arXiv:2412.09237*, 2024.
- Liu, Y., Liu, W., Gu, X., He, A., Wang, W., and Zhang, Y. Popsim: Social network simulation for social media popularity prediction. *arXiv preprint arXiv:2512.02533*, 2025a.
- Liu, Y., Liu, W., Gu, X., Wang, W., Luo, J., and Zhang, Y. Rumorsphere: A framework for million-scale agent-based dynamic simulation of rumor propagation. *arXiv preprint arXiv:2509.02172*, 2025b.
- Luo, M., Chen, F., Hu, D., Zhang, Y., Liang, J., and Feng, J. No fear of heterogeneity: Classifier calibration for federated learning with non-iid data. *Advances in Neural Information Processing Systems*, 34:5972–5984, 2021.
- Ma, Y., Xie, Z., Wang, J., Chen, K., and Shou, L. Continual federated learning based on knowledge distillation. In *Proceedings of the Thirty-First International Joint Conference on Artificial Intelligence*, volume 3, 2022.
- Ma’sum, M. A., Pratama, M., Ramasamy, S., Liu, L., Habibullah, H., and Kowalczyk, R. Pip: Prototypes-injected prompt for federated class incremental learning. In *Proceedings of the 33rd ACM International Conference on Information and Knowledge Management*, pp. 1670–1679, 2024.
- McDonnell, M. D., Gong, D., Parvaneh, A., Abbasnejad, E., and van den Hengel, A. Ranpac: Random projections and pre-trained models for continual learning. *Advances in Neural Information Processing Systems*, 36, 2024.
- McMahan, B., Moore, E., Ramage, D., Hampson, S., and y Arcas, B. A. Communication-efficient learning of deep networks from decentralized data. In *Artificial intelligence and statistics*, pp. 1273–1282. PMLR, 2017.
- Mourtada, J. and Rosasco, L. An elementary analysis of ridge regression with random design. *Comptes Rendus. Mathématique*, 360(G9):1055–1063, 2022.
- Pan, P., Swaroop, S., Immer, A., Eschenhagen, R., Turner, R., and Khan, M. E. E. Continual deep learning by functional regularisation of memorable past. *Advances in Neural Information Processing Systems*, 33:4453–4464, 2020.
- Peng, L., Elenter, J., Agterberg, J., Ribeiro, A., and Vidal, R. Icl-tsvd: Bridging theory and practice in continual learning with pre-trained models. *arXiv preprint arXiv:2410.00645*, 2024.
- Qi, D., Zhao, H., and Li, S. Better generative replay for continual federated learning. In *The Eleventh International Conference on Learning Representations*.
- Shim, D., Mai, Z., Jeong, J., Sanner, S., Kim, H., and Jang, J. Online class-incremental continual learning with adversarial shapley value. In *Proceedings of the AAAI Conference on Artificial Intelligence*, volume 35, pp. 9630–9638, 2021.

- Simon, C., Koniusz, P., and Harandi, M. On learning the geodesic path for incremental learning. In *Proceedings of the IEEE/CVF conference on Computer Vision and Pattern Recognition*, pp. 1591–1600, 2021.
- Smith, J. S., Karlinsky, L., Gutta, V., Cascante-Bonilla, P., Kim, D., Arbelles, A., Panda, R., Feris, R., and Kira, Z. Coda-prompt: Continual decomposed attention-based prompting for rehearsal-free continual learning. In *Proceedings of the IEEE/CVF Conference on Computer Vision and Pattern Recognition*, pp. 11909–11919, 2023.
- Tan, A. Z., Feng, S., and Yu, H. Fl-clip: Bridging plasticity and stability in pre-trained federated class-incremental learning models. In *2024 IEEE International Conference on Multimedia and Expo (ICME)*, pp. 1–6. IEEE, 2024.
- Tan, Y., Long, G., Ma, J., Liu, L., Zhou, T., and Jiang, J. Federated learning from pre-trained models: A contrastive learning approach. *Advances in neural information processing systems*, 35:19332–19344, 2022.
- Tran, M.-T., Le, T., Le, X.-M., Harandi, M., and Phung, D. Text-enhanced data-free approach for federated class-incremental learning. In *Proceedings of the IEEE/CVF Conference on Computer Vision and Pattern Recognition*, pp. 23870–23880, 2024.
- Ulyanov, D., Vedaldi, A., and Lempitsky, V. Deep image prior. In *Proceedings of the IEEE conference on computer vision and pattern recognition*, pp. 9446–9454, 2018.
- Wainwright, M. J. *High-dimensional statistics: A non-asymptotic viewpoint*, volume 48. Cambridge university press, 2019.
- Wang, S., Fu, Y., Li, X., Lan, Y., Gao, M., et al. Dfrd: Data-free robustness distillation for heterogeneous federated learning. *Advances in Neural Information Processing Systems*, 36, 2024.
- Wang, Z., Zhang, Z., Ebrahimi, S., Sun, R., Zhang, H., Lee, C.-Y., Ren, X., Su, G., Perot, V., Dy, J., et al. Dualprompt: Complementary prompting for rehearsal-free continual learning. In *European Conference on Computer Vision*, pp. 631–648. Springer, 2022.
- Yang, X., Yu, H., Gao, X., Wang, H., Zhang, J., and Li, T. Federated continual learning via knowledge fusion: A survey. *IEEE Transactions on Knowledge and Data Engineering*, 36(8):3832–3850, 2024.
- Yoon, J., Jeong, W., Lee, G., Yang, E., and Hwang, S. J. Federated continual learning with weighted inter-client transfer. In *International Conference on Machine Learning*, pp. 12073–12086. PMLR, 2021.
- Yu, H., Yang, X., Gao, X., Kang, Y., Wang, H., Zhang, J., and Li, T. Personalized federated continual learning via multi-granularity prompt. In *Proceedings of the 30th ACM SIGKDD Conference on Knowledge Discovery and Data Mining*, pp. 4023–4034, 2024.
- Zhang, J., Chen, C., Zhuang, W., and Lyu, L. Target: Federated class-continual learning via exemplar-free distillation. In *Proceedings of the IEEE/CVF International Conference on Computer Vision*, pp. 4782–4793, 2023.
- Zhang, J., Duan, Y., Niu, S., Cao, Y., and Lim, W. Y. B. Enhancing federated domain adaptation with multi-domain prototype-based federated fine-tuning. *arXiv preprint arXiv:2410.07738*, 2024a.
- Zhang, J., Hua, Y., Cao, J., Wang, H., Song, T., Xue, Z., Ma, R., and Guan, H. Eliminating domain bias for federated learning in representation space. *Advances in Neural Information Processing Systems*, 36, 2024b.
- Zhang, L., Shen, L., Ding, L., Tao, D., and Duan, L.-Y. Fine-tuning global model via data-free knowledge distillation for non-iid federated learning. In *Proceedings of the IEEE/CVF conference on computer vision and pattern recognition*, pp. 10174–10183, 2022.
- Zhou, D.-W., Cai, Z.-W., Ye, H.-J., Zhan, D.-C., and Liu, Z. Revisiting class-incremental learning with pre-trained models: Generalizability and adaptivity are all you need. *International Journal of Computer Vision*, pp. 1–21, 2024a.
- Zhou, D.-W., Sun, H.-L., Ning, J., Ye, H.-J., and Zhan, D.-C. Continual learning with pre-trained models: A survey. *arXiv preprint arXiv:2401.16386*, 2024b.
- Zhou, D.-W., Sun, H.-L., Ye, H.-J., and Zhan, D.-C. Expandable subspace ensemble for pre-trained model-based class-incremental learning. In *Proceedings of the IEEE/CVF Conference on Computer Vision and Pattern Recognition*, pp. 23554–23564, 2024c.
- Zhou, D.-W., Wang, Q.-W., Qi, Z.-H., Ye, H.-J., Zhan, D.-C., and Liu, Z. Class-incremental learning: A survey. *IEEE Transactions on Pattern Analysis and Machine Intelligence*, 2024d.
- Zhu, Z., Hong, J., and Zhou, J. Data-free knowledge distillation for heterogeneous federated learning. In *International conference on machine learning*, pp. 12878–12889. PMLR, 2021.
- Zhuang, H., Weng, Z., Wei, H., Xie, R., Toh, K.-A., and Lin, Z. Acil: Analytic class-incremental learning with absolute memorization and privacy protection. *Advances in Neural Information Processing Systems*, 35:11602–11614, 2022.

A. Proof of Proposition 3.1

Proposition 3.1. For each task \mathcal{T}_t ,

$$\hat{\mathbf{G}}_t = \sum_{i=1}^{c_t} \left[\frac{n_t^{(i)} - 1}{K - 1} \sum_{k=1}^K \frac{\mathbf{C}_{t,k}^{(i)} \mathbf{C}_{t,k}^{(i)\top}}{n_{t,k}^{(i)}} - \frac{n_t^{(i)} - K}{n_t^{(i)}(K - 1)} \left(\sum_{k=1}^K \mathbf{C}_{t,k}^{(i)} \right) \left(\sum_{k=1}^K \mathbf{C}_{t,k}^{(i)} \right)^\top \right], \quad (13)$$

is an unbiased plug-in estimator of the global gram matrix \mathbf{G}_t when global feature set $\Omega = \{(\Phi(x), y) \mid (x, y) \in \cup_{k=1}^K \mathcal{D}_{t,k}\}$ is i.i.d. Here, $\mathbf{C}_{t,k}^{(i)}$ denotes the i -th column of $\mathbf{C}_{t,k}$ and $n_t^{(i)}$ denotes the total number of data samples from class i in stage t , and $n_{t,k}^{(i)}$ denotes the number of samples from class i for client k at stage t .

Proof. For simplicity, we omit the subscript t in the proof. Under the i.i.d assumption of the global feature set $\{(\Phi(x), y) \mid (x, y) \in \cup_{k=1}^K \mathcal{D}_k\}$, and letting $n_k^{(i)}$ denote the total number of data samples from class i in client k , we have:

$$\mathbb{E}[\mathbf{C}_k^{(i)}] = \sum_{(x,i) \in D_k} \mathbb{E}[\Phi(x)] := n_k^{(i)} \mu^{(i)}, \quad \mathbb{D}[\mathbf{C}_k^{(i)}] = \sum_{(x,i) \in D_k} \mathbb{D}[\Phi(x)] := n_k^{(i)} \Sigma^{(i)}. \quad (14)$$

Here, $\mu^{(i)}$ and $\Sigma^{(i)}$ are the class-wise mean and covariance of the global feature set Ω . Since $\mathbf{G} = \sum_{i=1}^c \mathbf{G}^{(i)} = \sum_{i=1}^c \sum_{k=1}^K \mathbf{G}_k^{(i)}$, we have $\mathbb{E}[\mathbf{G}] = \sum_{i=1}^c \mathbb{E}[\mathbf{G}^{(i)}]$ and

$$\begin{aligned} \mathbb{E}[\mathbf{G}^{(i)}] &= \sum_{k=1}^K \mathbb{E}[\mathbf{G}_k^{(i)}] = \sum_{k=1}^K \mathbb{E}[\mathbf{X}_k^{(i)\top} \mathbf{X}_k^{(i)}] = \sum_{k=1}^K \sum_{(x,i) \in D_k} \mathbb{E}[\Phi(x)\Phi(x)^\top] \\ &= \sum_{k=1}^K (n_k^{(i)} \mu^{(i)} \mu^{(i)\top} + n_k^{(i)} \Sigma^{(i)}) = n^{(i)} \mu^{(i)} \mu^{(i)\top} + n^{(i)} \Sigma^{(i)} \end{aligned} \quad (15)$$

For clarity in the proof, we expand $\mathbb{E}[\hat{\mathbf{G}}]$ and divide it into several parts as follows:

$$\begin{aligned} \mathbb{E}[\hat{\mathbf{G}}] &= \sum_{i=1}^c \mathbb{E}[\hat{\mathbf{G}}^{(i)}] = \sum_{i=1}^c \left[\frac{n^{(i)} - 1}{K - 1} A_{1,i} - \frac{n^{(i)} - K}{n^{(i)}(K - 1)} A_{2,i} \right], \\ \text{where } A_{1,i} &= \sum_{k=1}^K \frac{\mathbb{E}[\mathbf{C}_k^{(i)} \mathbf{C}_k^{(i)\top}]}{n_k^{(i)}}, \quad A_{2,i} = \mathbb{E} \left[\left(\sum_{k=1}^K \mathbf{C}_k^{(i)} \right) \left(\sum_{k=1}^K \mathbf{C}_k^{(i)} \right)^\top \right]. \end{aligned} \quad (16)$$

To proceed, we compute each term in above equation separately:

$$\begin{aligned} A_{1,i} &= \sum_{k=1}^K \frac{\mathbb{E}[\mathbf{C}_k^{(i)} \mathbf{C}_k^{(i)\top}]}{n_k^{(i)}} = \sum_{k=1}^K \frac{\mathbb{E}[\mathbf{C}_k^{(i)}] \mathbb{E}[\mathbf{C}_k^{(i)}]^\top + \mathbb{D}[\mathbf{C}_k^{(i)}]}{n_k^{(i)}} \\ &= \sum_{k=1}^K (n_k^{(i)} \mu^{(i)} \mu^{(i)\top} + \Sigma^{(i)}) = n^{(i)} \mu^{(i)} \mu^{(i)\top} + K \Sigma^{(i)} \end{aligned} \quad (17)$$

$$\begin{aligned} A_{2,i} &= \mathbb{E} \left[\left(\sum_{k=1}^K \mathbf{C}_k^{(i)} \right) \left(\sum_{k=1}^K \mathbf{C}_k^{(i)} \right)^\top \right] = \mathbb{E} \left[\sum_{k=1}^K \mathbf{C}_k^{(i)} \right] \mathbb{E} \left[\sum_{k=1}^K \mathbf{C}_k^{(i)} \right]^\top + \mathbb{D} \left[\sum_{k=1}^K \mathbf{C}_k^{(i)} \right] \\ &= \left(\sum_{k=1}^K n_k^{(i)} \mu^{(i)} \right) \left(\sum_{k=1}^K n_k^{(i)} \mu^{(i)} \right)^\top + \sum_{k=1}^K n_k^{(i)} \Sigma^{(i)} = (n^{(i)})^2 \mu^{(i)} \mu^{(i)\top} + n^{(i)} \Sigma^{(i)} \end{aligned} \quad (18)$$

Therefore, by substituting $A_{1,i}$ and $A_{2,i}$ back into the equation for $\mathbb{E}[\hat{\mathbf{G}}]$, we get:

$$\begin{aligned} \mathbb{E}[\hat{\mathbf{G}}] &= \sum_{i=1}^c \left[\frac{n^{(i)} - 1}{K - 1} (n^{(i)} \mu^{(i)} \mu^{(i)\top} + K \Sigma^{(i)}) - \frac{n^{(i)} - K}{n^{(i)}(K - 1)} ((n^{(i)})^2 \mu^{(i)} \mu^{(i)\top} + n^{(i)} \Sigma^{(i)}) \right] \\ &= \sum_{i=1}^c \left[n^{(i)} \mu^{(i)} \mu^{(i)\top} + n^{(i)} \Sigma^{(i)} \right] = \sum_{i=1}^c \mathbb{E}[\mathbf{G}^{(i)}] = \mathbb{E}[\mathbf{G}] \end{aligned} \quad (19)$$

□

B. i.i.d. assumption of global feature set Ω

In FCIL, **non-i.i.d. refers to label skew setting** where the label distributions $P_k(y)$ vary across clients, while the conditional distribution $P_k(x|y)$ remains the same for all clients (Zhang et al., 2023; Tran et al., 2024). Given the shared backbone Φ , the conditional feature distribution $P_k(\Phi(x)|y)$ is also uniform across clients. Therefore, the global feature set $\Omega = \{(\Phi(x), y) \mid (x, y) \in \cup_{k=1}^K \mathcal{D}_k\}$ follows a mixture distribution:

$$P_\Omega(\Phi(X), Y) = \sum_{k=1}^K w_k P_k(\Phi(X), Y) = P(\Phi(X)|Y) \sum_{k=1}^K w_k P_k(Y) = P(\Phi(X)|Y) P_{avg}(Y), \quad (20)$$

where w_k is the proportion of data from client k ($w_k = \frac{|D_k|}{|\cup_{k=1}^K D_k|}$), and $P_{avg}(Y)$ is the global average label distribution across all data.

The non-i.i.d. nature of the clients ($P_k(Y)$) only influences the shape of the final mixture distribution P_Ω (via $P_{avg}(Y)$), but it does not prevent samples drawn from Ω from being identically distributed according to P_Ω . Therefore, the i.i.d. assumption of Ω in Proposition 3.1 (following the single mixture distribution P_Ω) is valid within the label skew setting (non-i.i.d. in FCIL).

This explains why STSA-E shows strong robustness and comparable performance to STSA across varying data heterogeneity in our experiments.

C. Estimation Guarantee of STSA-E

Notation: Let $\|\cdot\|_2$ denote the spectral norm, $\|\cdot\|_F$ represent the Frobenius norm, \mathbb{E} indicate the expectation operator, \mathbb{D} signify the variance operator, $\mathbf{0}$ be the zero vector, \mathbf{I}_M denote the M -dimensional identity matrix, and $\text{tr}(\cdot)$ represent the matrix trace operation. We consider a noisy linear regression model and let n represent the total number of collected samples until stage t , that is, $n = \sum_{i=1}^t n_i$ and $c_{\text{joint}} = \sum_{i=1}^t c_i$. In the subsequent discussion, we assume that, through sufficient continual learning and accumulation, the number of samples n exceeds the feature dimension M , i.e., $n > M$. Specifically, we assume there exist ground-truth weight matrix $\mathbf{W}_t^0 \in \mathbb{R}^{M \times c_{\text{joint}}}$ and noise $\mathcal{E}_{\text{joint}} \in \mathbb{R}^{n \times c_{\text{joint}}}$ satisfying

$$\mathbf{Y}_{\text{joint}} = \mathbf{X}_{\text{joint}} \mathbf{W}_t^0 + \mathcal{E}_{\text{joint}}. \quad (21)$$

For each task \mathcal{T}_t , and for every $i \in \{1, \dots, c_t\}$, we assume:

Assumption 1 (Data Structure). $\|\mathbf{X}_t\|_F \leq \sqrt{n_t} C_X$, $\text{tr}(\Sigma_t^{(i)}) \leq C_\Sigma$ and $\|\mu_t^{(i)}\|_2^2 \leq C_\mu$ for some constants $C_X, C_\Sigma, C_\mu > 0$, where $\mu_t^{(i)}$ and $\Sigma_t^{(i)}$ are the class-wise mean and covariance of the global feature set Ω at stage t .

Assumption 2 (Class Balance). There exists a constant $0 < C \ll c_t$ such that $c_t \sum_{i=1}^{c_t} n_t^{(i)2} \leq C n_t^2$.

Assumption 3 (Stability). $\|\mathbf{W}_t^0\|_F \leq \sqrt{M} r$ for some constant $r > 0$.

Assumption 4 (Noise). The i -th row of noise satisfies the following conditions: $\mathbb{E}(\mathcal{E}_{\text{joint},i}^\top) = \mathbf{0}$, $\mathbb{E}(\mathcal{E}_{\text{joint},i}^\top \mathcal{E}_{\text{joint},i}) = \sigma^2 \mathbf{I}_M$ and $\mathcal{E}_{\text{joint}}$ is independent of $\mathbf{X}_{\text{joint}}$.

These four assumptions are mild in statistical learning theory and are consistent with (and often weaker than) those in related theoretical works (Ding et al., 2024; Peng et al., 2024). We formalize these assumptions to ensure theoretical rigor while maintaining practical relevance. Here, we further explain the rationality of these assumptions:

Assumptions 1 (Data Structure) and 3 (Stability) are common boundedness conditions in theoretical analyses (Peng et al., 2024). They simply ensure that feature and weight norms remain finite, which naturally holds in real-world scenarios. **Assumption 2 (Class Balance)** is a mild and flexible condition for global class distribution (considering all data across all clients): it does not require equal sample sizes across classes but only rules out extreme imbalance where one class dominates almost all samples (i.e., $\sum n_t^{(i)2} \ll n_t^2$). This aligns with practical FCIL settings, where the global class distribution typically includes multiple classes with reasonable diversity. **Assumption 4 (Noise)** generalizes standard noise models in statistical learning. We only require zero-mean, homoscedastic, and feature-independent noise. This condition is less restrictive than many prior works that assume Gaussianity (Ding et al., 2024; Peng et al., 2024), enabling broader applicability to real-world noise patterns without imposing stringent distributional constraints.

Proposition 3.2. Under Assumption 1-2, when considering $\hat{\mathbf{G}}_t$ as described in Proposition 3.1, we obtain the following results:

$$\mathbb{E} \left\| \hat{\mathbf{G}}_t - \mathbf{G}_t \right\|_F^2 \leq C' C_\Sigma^2 \left(\frac{K+1}{K-1} \right)^2 n_t^2 = O\left(\left(\frac{K+1}{K-1} \right)^2 n_t^2 \right), \quad (22)$$

where C' represents a constant that is independent of (n_t, K) .

Proof. For simplicity, we omit the subscript t in the proof.

$$\begin{aligned} \left\| \hat{\mathbf{G}} - \mathbf{G} \right\|_F^2 &\leq c \sum_{i=1}^c \left\| \hat{\mathbf{G}}^{(i)} - \mathbf{G}^{(i)} \right\|_F^2 \\ &= c \sum_{i=1}^c \left\| \frac{n^{(i)} - 1}{K-1} \sum_{k=1}^K \frac{\mathbf{C}_k^{(i)} \mathbf{C}_k^{(i)\top}}{n_k^{(i)}} - \frac{n^{(i)} - K}{n^{(i)}(K-1)} \left(\sum_{k=1}^K \mathbf{C}_k^{(i)} \right) \left(\sum_{k=1}^K \mathbf{C}_k^{(i)} \right)^\top - \sum_{k=1}^K \mathbf{X}_k^{(i)\top} \mathbf{X}_k^{(i)} \right\|_F^2 \\ &\leq (K+1)c \sum_{i=1}^c \left(\left(\frac{n^{(i)} - K}{K-1} \right)^2 A_1^{(i)} + \left(\frac{n^{(i)} - 1}{K-1} \right)^2 \sum_{k=1}^K A_{2,k}^{(i)} \right), \end{aligned} \quad (23)$$

where $A_1^{(i)}$ measures global random error, $A_{2,k}^{(i)}$ measures local random error,

$$A_1^{(i)} = \left\| \mathbf{X}^{(i)\top} \mathbf{X}^{(i)} - \frac{1}{n^{(i)}} \left(\sum_{k=1}^K \mathbf{C}_k^{(i)} \right) \left(\sum_{k=1}^K \mathbf{C}_k^{(i)} \right)^\top \right\|_F^2, \quad A_{2,k}^{(i)} = \left\| \mathbf{X}_k^{(i)\top} \mathbf{X}_k^{(i)} - \frac{1}{n_k^{(i)}} \mathbf{C}_k^{(i)} \mathbf{C}_k^{(i)\top} \right\|_F^2. \quad (24)$$

Noticing that the forms of these two terms are identical (except for the constants in front), we can use Lemma 3.5 to analyze them, which we assume that $\mathbb{E}[\mathbf{C}_k^{(i)}] := n_k^{(i)} \mu^{(i)}$, $\mathbb{D}[\mathbf{C}_k^{(i)}] := n_k^{(i)} \Sigma^{(i)}$. Then we have,

$$\mathbb{E}[A_1^{(i)}] \leq \frac{n^{(i)} - 1}{n^{(i)}} \text{tr}(\Sigma^{(i)})^2, \quad \mathbb{E}[A_{2,k}^{(i)}] \leq \frac{n_k^{(i)} - 1}{n_k^{(i)}} \text{tr}(\Sigma^{(i)})^2, \quad (25)$$

then we have

$$\begin{aligned} \mathbb{E} \left\| \hat{\mathbf{G}} - \mathbf{G} \right\|_F^2 &\leq C_\Sigma^2 (K+1)c \sum_{i=1}^c \left(\left(\frac{n^{(i)} - K}{K-1} \right)^2 \frac{n^{(i)} - 1}{n^{(i)}} + \left(\frac{n^{(i)} - 1}{K-1} \right)^2 \sum_{k=1}^K \frac{n_k^{(i)} - 1}{n_k^{(i)}} \right) \\ &= C'' C_\Sigma^2 \frac{(K+1)^2}{(K-1)^2} c \sum_{i=1}^c n^{(i)2} \leq C' C_\Sigma^2 \frac{(K+1)^2}{(K-1)^2} n^2 = O\left(\left(\frac{K+1}{K-1} \right)^2 n^2 \right), \end{aligned} \quad (26)$$

where we scale some constants such as $\frac{n^{(i)}}{n^{(i)}-1}$ as C'' , which is a product factor of a finite number of quantities approximately equal to 1. Moreover, we utilize our class balanced condition to get another constant C' . \square

Remark. Proposition 3.2 indicates that the error between $\hat{\mathbf{G}}_t$ and \mathbf{G}_t is highly sensitive to small values of K , but the sensitivity diminishes as K increases.

After quantitatively analyzing the relationship between $\hat{\mathbf{G}}_t$ and \mathbf{G}_t , we can use Proposition 3.1 and 3.2 to further explore more profound theoretical properties between $\mathbf{W}_t = \left(\hat{\mathbf{G}}_{1:t} + \gamma \mathbf{I} \right)^{-1} \mathbf{C}_{1:t}$ and $\mathbf{W}^* = \left(\mathbf{G}_{1:t} + \gamma \mathbf{I} \right)^{-1} \mathbf{C}_{1:t}$.

Theorem 3.3 (STSA-E plug-in error). Under Assumption 1-2, with high probability, we have

$$\frac{1}{n} \mathbb{E} \left\| \mathbf{X}_{\text{joint}} \mathbf{W}_t - \mathbf{X}_{\text{joint}} \mathbf{W}^* \right\|_F \leq \frac{C'' C_{\mathbf{X}} (C_\Sigma)^{3/2} C_\mu^{1/2} \frac{K+1}{K-1} t}{n \left(\frac{\gamma^2}{n^2} + C' \right)} = O\left(\frac{\frac{K+1}{K-1} t}{n \left(\frac{\gamma^2}{n^2} + 1 \right)} \right), \quad (27)$$

where C', C'' are the constants that are independent of (n, t, K, γ) .

Proof. Firstly, we expand the term in expectation:

$$\begin{aligned}
 \|\mathbf{X}_{\text{joint}} \mathbf{W}_t - \mathbf{X}_{\text{joint}} \mathbf{W}^*\|_F &\leq \|\mathbf{X}_{\text{joint}}\|_F \|\mathbf{W}_t - \mathbf{W}^*\|_F \\
 &= \|\mathbf{X}_{\text{joint}}\|_F \left\| \left(\hat{\mathbf{G}}_{1:t} + \gamma \mathbf{I} \right)^{-1} - \left(\mathbf{G}_{1:t} + \gamma \mathbf{I} \right)^{-1} \right\|_F \mathbf{C}_{1:t} \|_F \\
 &= \|\mathbf{X}_{\text{joint}}\|_F \left\| \left(\hat{\mathbf{G}}_{1:t} + \gamma \mathbf{I} \right)^{-1} \left(\mathbf{G}_{1:t} - \hat{\mathbf{G}}_{1:t} \right) \left(\mathbf{G}_{1:t} + \gamma \mathbf{I} \right)^{-1} \mathbf{C}_{1:t} \right\|_F \\
 &\leq \|\mathbf{X}_{\text{joint}}\|_F \left\| \left(\hat{\mathbf{G}}_{1:t} + \gamma \mathbf{I} \right)^{-1} \right\|_2 \|\mathbf{G}_{1:t} - \hat{\mathbf{G}}_{1:t}\|_F \left\| \left(\mathbf{G}_{1:t} + \gamma \mathbf{I} \right)^{-1} \right\|_2 \|\mathbf{C}_{1:t}\|_F \\
 &\leq \frac{\|\mathbf{X}_{\text{joint}}\|_F \|\mathbf{C}_{1:t}\|_F \|\mathbf{G}_{1:t} - \hat{\mathbf{G}}_{1:t}\|_F}{\gamma^2 + C'n^2} \leq \frac{C_{\mathbf{X}} \sqrt{tn} \|\mathbf{C}_{1:t}\|_F}{\gamma^2 + C'n^2} \sum_{i=1}^t \|\mathbf{G}_i - \hat{\mathbf{G}}_i\|_F, \tag{28}
 \end{aligned}$$

where the first inequality is based on the property $\|AB\|_F \leq \|A\|_F \|B\|_F$, and the second inequality follows from $\|AB\|_F \leq \|A\|_2 \|B\|_F$. The second equality holds because $A^{-1} - B^{-1} = A^{-1}(B - A)B^{-1}$.

Regarding the third inequality, we consider $\left\| \left(\mathbf{G}_{1:t} + \gamma \mathbf{I} \right)^{-1} \right\|_2$ firstly. Notice that

$$\left\| \left(\mathbf{G}_{1:t} + \gamma \mathbf{I} \right)^{-1} \right\|_2 = \frac{1}{\min_i \lambda_i + \gamma} \quad \text{where } \lambda_i \text{ is the } i\text{-th eigenvalue of } \mathbf{G}_{1:t}, \tag{29}$$

Where $\mathbf{G}_{1:t}$ is, in fact, the sum of the outer products of n vectors. According to Lemma 3.7, when the number of vectors n exceeds the dimension M , with high probability, we can derive that $\min_i \lambda_i \geq O(n)$. The analysis result for $\left\| \left(\hat{\mathbf{G}}_{1:t} + \gamma \mathbf{I} \right)^{-1} \right\|_2$ is similar by Lemma 3.7-3.8. Therefore, we can postulate the existence of a certain positive constant C' such that

$$\left\| \left(\mathbf{G}_{1:t} + \gamma \mathbf{I} \right)^{-1} \right\|_2 \cdot \left\| \left(\hat{\mathbf{G}}_{1:t} + \gamma \mathbf{I} \right)^{-1} \right\|_2 \leq \frac{1}{C'n^2 + \gamma^2}. \tag{30}$$

Regarding the fourth inequality, it is derived by considering the Cauchy inequality and the fact that $\|\mathbf{X}_{\text{joint}}\|_F \leq \sum_{i=1}^t \|\mathbf{X}_i\|_F$, where $\mathbf{X}_{\text{joint}}$ is the matrix obtained by concatenating the matrices \mathbf{X}_i .

By Cauchy inequality, we have

$$\mathbb{E} \left[\|\mathbf{C}_{1:t}\|_F \sum_{i=1}^t \|\mathbf{G}_i - \hat{\mathbf{G}}_i\|_F \right] = \sum_{i=1}^t \mathbb{E} \left[\|\mathbf{C}_{1:t}\|_F \|\mathbf{G}_i - \hat{\mathbf{G}}_i\|_F \right] \leq \sum_{i=1}^t \sqrt{\mathbb{E} \left[\|\mathbf{C}_{1:t}\|_F^2 \right] \mathbb{E} \left[\|\mathbf{G}_i - \hat{\mathbf{G}}_i\|_F^2 \right]} \tag{31}$$

Then, we bound $\mathbb{E} \left[\|\mathbf{C}_{1:t}\|_F^2 \right]$,

$$\begin{aligned}
 \mathbb{E} \left[\|\mathbf{C}_{1:t}\|_F^2 \right] &\leq \mathbb{E} \left[\sum_{i=1}^t \mathbf{C}_t \|\mathbf{C}_t\|_F^2 \right] \leq \mathbb{E} \left[\sum_{i=1}^t \|\mathbf{C}_t\|_F^2 \right] \leq t \sum_{i=1}^t \mathbb{E} \left[\|\mathbf{C}_t\|_F^2 \right] \\
 &= t \sum_{i=1}^t \mathbb{E} \text{tr} \left(\mathbf{X}_i^\top \mathbf{Y}_i \mathbf{Y}_i^\top \mathbf{X}_i \right) = t \sum_{i=1}^t \mathbb{E} \text{tr} \left(\mathbf{Y}_i \mathbf{Y}_i^\top \mathbf{X}_i \mathbf{X}_i^\top \right) \\
 &= t \sum_{i=1}^t \sum_{j=1}^{c_i} n_i^{(j)} \left(\mu_i^{(j)\top} \mu_i^{(j)} + \text{tr} \left(\Sigma^{(j)} \right) \right) \leq C_{\Sigma} C_{\mu} t n. \tag{32}
 \end{aligned}$$

By taking the result in Proposition 3.2, and combining the above parts, we have

$$\mathbb{E} \|\mathbf{X}_{\text{joint}} \mathbf{W}_t - \mathbf{X}_{\text{joint}} \mathbf{W}^*\|_F \leq \frac{C_{\mathbf{X}} C_{\Sigma}^{1/2} C_{\mu}^{1/2} t}{\left(\frac{\gamma^2}{n} + C'n \right)} \sum_{i=1}^t \sqrt{\mathbb{E} \left[\|\mathbf{G}_i - \hat{\mathbf{G}}_i\|_F^2 \right]} \leq \frac{C'' C_{\mathbf{X}} (C_{\Sigma})^{3/2} C_{\mu}^{1/2} \frac{K+1}{K-1} t}{\frac{\gamma^2}{n^2} + C'}, \tag{33}$$

where C'' is the constant in Proposition 3.2. □

Remark. Theorem 3.3 establishes that the plug-in error decreases as the average per-stage sample size $\frac{n}{t}$ increases.

Corollary 3.4 (Estimation error). *Under the Assumption 1-4, with high probability, we have*

$$\frac{1}{n} \mathbb{E} \|\mathbf{X}_{\text{joint}} \mathbf{W}_t - \mathbf{Y}_{\text{joint}}\|_F \leq \frac{C'' C_{\mathbf{X}} (C_{\Sigma})^{3/2} C_{\mu}^{1/2} \frac{K+1}{K-1} t}{n \left(\frac{\gamma^2}{n^2} + C' \right)} + \frac{MRC_{\mathbf{X}} + \sigma}{\sqrt{n}}, \quad (34)$$

where C', C'' are the constants that are independent of (n, t, K, γ) .

Proof. Consider the error decomposition:

$$\begin{aligned} \frac{1}{n} \mathbb{E} \|\mathbf{X}_{\text{joint}} \mathbf{W}_t - \mathbf{Y}_{\text{joint}}\|_F &\leq \frac{1}{n} \mathbb{E} \|\mathbf{X}_{\text{joint}} \mathbf{W}_t - \mathbf{X}_{\text{joint}} \mathbf{W}^*\|_F + \frac{1}{n} \mathbb{E} \|\mathbf{X}_{\text{joint}} \mathbf{W}^* - \mathbf{Y}_{\text{joint}}\|_F \\ &\leq \frac{1}{n} \mathbb{E} \|\mathbf{X}_{\text{joint}} \mathbf{W}_t - \mathbf{X}_{\text{joint}} \mathbf{W}^*\|_F + \frac{1}{n} \sqrt{\mathbb{E} \|\mathbf{X}_{\text{joint}} \mathbf{W}^* - \mathbf{Y}_{\text{joint}}\|_F^2}, \end{aligned} \quad (35)$$

where the first term has been analyzed in Theorem 3.3, and we introduce Lemma 3.6 to analyze the second term. Then

$$\frac{1}{n} \mathbb{E} \|\mathbf{X}_{\text{joint}} \mathbf{W}_t - \mathbf{X}_{\text{joint}} \mathbf{W}^*\|_F \leq \frac{C'' C_{\mathbf{X}} (C_{\Sigma})^{3/2} C_{\mu}^{1/2} \frac{K+1}{K-1} t}{n \left(\frac{\gamma^2}{n^2} + C' \right)} = O \left(\frac{\frac{K+1}{K-1} t}{n \left(\frac{\gamma^2}{n^2} + 1 \right)} \right). \quad (36)$$

$$\frac{1}{n} \sqrt{\mathbb{E} \|\mathbf{X}_{\text{joint}} \mathbf{W}^* - \mathbf{Y}_{\text{joint}}\|_F^2} \leq \frac{MRC_{\mathbf{X}} + \sigma}{\sqrt{n}} = O \left(\frac{1}{\sqrt{n}} \right). \quad (37)$$

Combing this two parts, we can proof the Corollary 3.4. \square

Remark. The most significant implication of Corollary 3.4 lies in the rate analysis: our STSA-E incurs an estimation efficiency loss of order $O(tn^{-1})$, whereas the oracle estimator achieves the standard rate $O(n^{-1/2})$. Crucially, when $t \ll \sqrt{n}$ (a mild scaling condition), the efficiency loss becomes asymptotically negligible. Thus, our method achieves comparable statistical performance to the oracle approach while requiring substantially lower communication overhead, establishing a favorable trade-off between precision and resource efficiency.

Lemma 3.5. *Let $\mathbf{x}_1, \mathbf{x}_2, \dots, \mathbf{x}_n$ be i.i.d. random vectors such that $\mathbf{x}_i \sim N(\mu, \Sigma)$ for $i = 1, 2, \dots, n$, where $\Sigma = (\sigma_{ij})_{i,j=1}^d$ is a $d \times d$ positive covariance matrix. Define the matrix $\mathbf{M} = \sum_{i=1}^n \mathbf{x}_i \mathbf{x}_i^\top - \frac{1}{n} (\sum_{i=1}^n \mathbf{x}_i) (\sum_{i=1}^n \mathbf{x}_i)^\top$. Then, the expected value of the Frobenius norm of \mathbf{M} satisfies the following equality:*

$$\mathbb{E} [\|\mathbf{M}\|_F^2] = \frac{n-1}{n} \text{tr}(\Sigma)^2.$$

Proof. Without loss of generality, we assume that $\mu = \mathbf{0}$.

By definition of Frobenius norm, we have $\mathbb{E} [\|\mathbf{M}\|_F^2] = \mathbb{E} [\text{tr}(\mathbf{M}^2)]$, then we expand \mathbf{M}^2 obtain,

$$\begin{aligned} \mathbf{M}^2 &= \left(\sum_{i=1}^n \mathbf{x}_i \mathbf{x}_i^\top - \frac{1}{n} \sum_{i=1}^n \sum_{j=1}^n \mathbf{x}_i \mathbf{x}_j^\top \right) \left(\sum_{k=1}^n \mathbf{x}_k \mathbf{x}_k^\top - \frac{1}{n} \sum_{k=1}^n \sum_{l=1}^n \mathbf{x}_k \mathbf{x}_l^\top \right) \\ &= \sum_{i=1}^n \sum_{k=1}^n (\mathbf{x}_i \mathbf{x}_i^\top) (\mathbf{x}_k \mathbf{x}_k^\top) - \frac{2}{n} \sum_{i=1}^n \sum_{k=1}^n \sum_{l=1}^n (\mathbf{x}_i \mathbf{x}_i^\top) (\mathbf{x}_k \mathbf{x}_l^\top) + \frac{1}{n^2} \sum_{i=1}^n \sum_{j=1}^n \sum_{k=1}^n \sum_{l=1}^n (\mathbf{x}_i \mathbf{x}_j^\top) (\mathbf{x}_k \mathbf{x}_l^\top). \end{aligned} \quad (38)$$

(1). We compute $\mathbb{E} [\text{tr}(\sum_{i=1}^n \sum_{k=1}^n (\mathbf{x}_i \mathbf{x}_i^\top) (\mathbf{x}_k \mathbf{x}_k^\top))]$. Since \mathbf{x}_i are independent and $\mathbb{E} [\mathbf{x}_i \mathbf{x}_j^\top] = \begin{cases} \Sigma, & i = j \\ \mathbf{0}, & i \neq j \end{cases}$, we have:

$$\mathbb{E} \left[\text{tr} \left(\sum_{i=1}^n \sum_{k=1}^n (\mathbf{x}_i \mathbf{x}_i^\top) (\mathbf{x}_k \mathbf{x}_k^\top) \right) \right] = \sum_{i=1}^n \mathbb{E} \left[\text{tr} \left((\mathbf{x}_i \mathbf{x}_i^\top)^2 \right) \right] + \sum_{i \neq k} \mathbb{E} \left[\text{tr} \left((\mathbf{x}_i \mathbf{x}_i^\top) (\mathbf{x}_k \mathbf{x}_k^\top) \right) \right], \quad (39)$$

then we calculate $\mathbb{E} \left[\text{tr} \left((\mathbf{x}_i \mathbf{x}_i^\top)^2 \right) \right]$. Let $\mathbf{x}_i = (x_{i1}, x_{i2}, \dots, x_{id})^\top$, $(\mathbf{x}_i \mathbf{x}_i^\top)_{jk} = x_{ij} x_{ik}$, and $\text{tr} \left((\mathbf{x}_i \mathbf{x}_i^\top)^2 \right) = \sum_{j=1}^d \sum_{k=1}^d (x_{ij} x_{ik})^2$. For a multivariate normal distribution $\mathbf{x} \sim N(\mathbf{0}, \Sigma)$, the fourth-moment formula is

$$\mathbb{E} [x_j x_k x_u x_v] = \sigma_{jk} \sigma_{uv} + \sigma_{ju} \sigma_{kv} + \sigma_{jv} \sigma_{ku}, \quad (40)$$

$$\mathbb{E} \left[\text{tr} \left((\mathbf{x}_i \mathbf{x}_i^\top)^2 \right) \right] = \sum_{j=1}^d \sum_{k=1}^d \mathbb{E} \left[(x_{ij} x_{ik})^2 \right] = \sum_{j=1}^d \sum_{k=1}^d (\sigma_{jk}^2 + \sigma_{jj} \sigma_{kk}). \quad (41)$$

Then we calculate $\mathbb{E} \left[\text{tr} \left((\mathbf{x}_i \mathbf{x}_i^\top) (\mathbf{x}_k \mathbf{x}_k^\top) \right) \right]$ for $i \neq k$. Since \mathbf{x}_i and \mathbf{x}_k are independent, $\mathbb{E} \left[(\mathbf{x}_i \mathbf{x}_i^\top) (\mathbf{x}_k \mathbf{x}_k^\top) \right] = \mathbb{E} [\mathbf{x}_i \mathbf{x}_i^\top] \mathbb{E} [\mathbf{x}_k \mathbf{x}_k^\top] = \Sigma^2$. Then we have $\mathbb{E} \left[\text{tr} \left((\mathbf{x}_i \mathbf{x}_i^\top) (\mathbf{x}_k \mathbf{x}_k^\top) \right) \right] = \text{tr} (\Sigma^2) = \sum_{j=1}^d \sum_{k=1}^d \sigma_{jk}^2$.

$$\sum_{i=1}^n \mathbb{E} \left[\text{tr} \left((\mathbf{x}_i \mathbf{x}_i^\top)^2 \right) \right] = n \sum_{j=1}^d \sum_{k=1}^d (\sigma_{jk}^2 + \sigma_{jj} \sigma_{kk}), \quad (42)$$

$$\sum_{i \neq k} \mathbb{E} \left[\text{tr} \left((\mathbf{x}_i \mathbf{x}_i^\top) (\mathbf{x}_k \mathbf{x}_k^\top) \right) \right] = n(n-1) \sum_{j=1}^d \sum_{k=1}^d \sigma_{jk}^2. \quad (43)$$

(2). We compute $E \left[\text{tr} \left(\frac{2}{n} \sum_{i=1}^n \sum_{k=1}^n \sum_{l=1}^n (\mathbf{x}_i \mathbf{x}_i^\top) (\mathbf{x}_k \mathbf{x}_l^\top) \right) \right]$. We consider different cases based on the indices. When $k = l$, we have terms related to $\mathbb{E} \left[(\mathbf{x}_i \mathbf{x}_i^\top) (\mathbf{x}_k \mathbf{x}_k^\top) \right]$. When $k \neq l$, we use the independence of \mathbf{x}_k and \mathbf{x}_l .

$$\mathbb{E} \left[\text{tr} \left(\frac{2}{n} \sum_{i=1}^n \sum_{k=1}^n \sum_{l=1}^n (\mathbf{x}_i \mathbf{x}_i^\top) (\mathbf{x}_k \mathbf{x}_l^\top) \right) \right] = \frac{2}{n} \left(n \sum_{j=1}^d \sum_{k=1}^d (\sigma_{jk}^2 + \sigma_{jj} \sigma_{kk}) + 2n(n-1) \sum_{j=1}^d \sum_{k=1}^d \sigma_{jk}^2 \right). \quad (44)$$

(3). We compute $E \left[\text{tr} \left(\frac{1}{n^2} \sum_{i=1}^n \sum_{j=1}^n \sum_{k=1}^n \sum_{l=1}^n (\mathbf{x}_i \mathbf{x}_j^\top) (\mathbf{x}_k \mathbf{x}_l^\top) \right) \right]$. By considering all possible combinations of indices and using the independence of \mathbf{x}_i and the properties of the normal distribution, we can show that

$$\begin{aligned} & \mathbb{E} \left[\text{tr} \left(\frac{1}{n^2} \sum_{i=1}^n \sum_{j=1}^n \sum_{k=1}^n \sum_{l=1}^n (\mathbf{x}_i \mathbf{x}_j^\top) (\mathbf{x}_k \mathbf{x}_l^\top) \right) \right] \\ &= \frac{1}{n^2} \left(n \sum_{j=1}^d \sum_{k=1}^d (\sigma_{jk}^2 + \sigma_{jj} \sigma_{kk}) + 4n(n-1) \sum_{j=1}^d \sum_{k=1}^d \sigma_{jk}^2 + (n^2 - 3n + 2) \sum_{j=1}^d \sum_{k=1}^d \sigma_{jk}^2 \right). \end{aligned} \quad (45)$$

After combining the above three parts, we have

$$\mathbb{E} \left[\text{tr} (\mathbf{M}^2) \right] = \frac{n-1}{n} \sum_{j=1}^d \sum_{k=1}^d \sigma_{jj} \sigma_{kk} = \frac{n-1}{n} \text{tr} (\Sigma)^2. \quad (46)$$

□

Lemma 3.6. Suppose that $\mathbf{Y} = \mathbf{X} \mathbf{W}_0 + \boldsymbol{\epsilon}$, where $\mathbf{Y} \in \mathbb{R}^{n \times c}$, $\mathbf{X} \in \mathbb{R}^{n \times M}$ is a random matrix whose rows $\mathbf{x}_i \sim \mathcal{N}(\boldsymbol{\mu}, \Sigma)$ for $i = 1, \dots, n$, $\mathbf{W}_0 \in \mathbb{R}^{M \times c}$, and $\boldsymbol{\epsilon} \in \mathbb{R}^{n \times c}$ is a noise matrix with $\mathbb{E}(\boldsymbol{\epsilon}) = \mathbf{0}$, $\mathbb{E}(\boldsymbol{\epsilon} \boldsymbol{\epsilon}^\top) = \sigma^2 \mathbf{I}_n$, and $\boldsymbol{\epsilon}$ is independent of \mathbf{X} . Let $\mathbf{W} = (\mathbf{X}^\top \mathbf{X} + \gamma \mathbf{I}_M)^{-1} \mathbf{X}^\top \mathbf{Y}$ be the ridge estimator. Then

$$\mathbb{E} \|\mathbf{X} \mathbf{W} - \mathbf{Y}\|_F^2 = \underbrace{\mathbb{E} \text{tr} \left[(\mathbf{H} - \mathbf{I}_n)^2 \mathbf{X} \mathbf{W}_0 \mathbf{W}_0^\top \mathbf{X}^\top \right]}_{\text{Bias}} + \underbrace{\text{tr} \left[\mathbb{E} (\mathbf{H} - \mathbf{I}_n)^2 \right]}_{\text{Variance}} \sigma^2. \quad (47)$$

where $\mathbf{H} = \mathbf{X} (\mathbf{X}^\top \mathbf{X} + \gamma \mathbf{I}_M)^{-1} \mathbf{X}^\top$. Besides, suppose further that: (1). The covariate matrix \mathbf{X} satisfies $\|\mathbf{X}\|_F \leq \sqrt{n} C_{\mathbf{X}}$ for some constant $C_{\mathbf{X}} > 0$. (2). The true parameter matrix \mathbf{W}_0 satisfies $\|\mathbf{W}_0\|_F \leq \sqrt{M} R$ for some constant $R > 0$. Then, we have:

$$\mathbb{E} \|\mathbf{X} \mathbf{W} - \mathbf{Y}\|_F^2 \leq n(M^2 R^2 C_{\mathbf{X}}^2 + \sigma^2). \quad (48)$$

Proof. First, substitute the expression of \mathbf{W} into $\mathbf{XW} - \mathbf{Y}$. Given $\mathbf{W} = (\mathbf{X}^\top \mathbf{X} + \gamma \mathbf{I}_M)^{-1} \mathbf{X}^\top \mathbf{Y}$ and $\mathbf{Y} = \mathbf{XW}_0 + \epsilon$, we denote $\mathbf{H} = \mathbf{X} (\mathbf{X}^\top \mathbf{X} + \gamma \mathbf{I}_M)^{-1} \mathbf{X}^\top$, then we have

$$\begin{aligned} \mathbf{XW} - \mathbf{Y} &= \mathbf{X} (\mathbf{X}^\top \mathbf{X} + \gamma \mathbf{I}_M)^{-1} \mathbf{X}^\top \mathbf{Y} - \mathbf{Y} = (\mathbf{H} - \mathbf{I}_n) \mathbf{Y} \\ &= (\mathbf{H} - \mathbf{I}_n) (\mathbf{XW}_0 + \epsilon) = (\mathbf{H} - \mathbf{I}_n) \mathbf{XW}_0 + (\mathbf{H} - \mathbf{I}_n) \epsilon. \end{aligned} \quad (49)$$

Consider $\mathbb{E} \|\mathbf{XW} - \mathbf{Y}\|_F^2 = \mathbb{E} \text{tr} [(\mathbf{XW} - \mathbf{Y})^\top (\mathbf{XW} - \mathbf{Y})]$, since $\mathbb{E}(\epsilon) = \mathbf{0}$ and ϵ is independent of \mathbf{X} , the cross-terms involving ϵ and \mathbf{XW}_0 will have zero expectation. Then

$$\begin{aligned} \mathbb{E} \|\mathbf{XW} - \mathbf{Y}\|_F^2 &= \mathbb{E} \text{tr} \left\{ [(\mathbf{H} - \mathbf{I}_n) \mathbf{XW}_0]^\top [(\mathbf{H} - \mathbf{I}_n) \mathbf{XW}_0] \right\} + \mathbb{E} \text{tr} \left\{ [(\mathbf{H} - \mathbf{I}_n) \epsilon]^\top [(\mathbf{H} - \mathbf{I}_n) \epsilon] \right\} \\ &= \underbrace{\mathbb{E} \text{tr} [(\mathbf{H} - \mathbf{I}_n)^2 \mathbf{XW}_0 \mathbf{W}_0^\top \mathbf{X}^\top]}_{\text{Bias}} + \underbrace{\text{tr} [\mathbb{E} (\mathbf{H} - \mathbf{I}_n)^2]}_{\text{Variance}} \sigma^2. \end{aligned} \quad (50)$$

Bias Term. Recall $\mathbf{H} = \mathbf{X} (\mathbf{X}^\top \mathbf{X} + \gamma \mathbf{I}_M)^{-1} \mathbf{X}^\top$. Using the identity: $\mathbf{H} - \mathbf{I}_n = \mathbf{X} \mathbf{X}^\top (\mathbf{X} \mathbf{X}^\top + \gamma \mathbf{I}_n)^{-1} - \mathbf{I}_n = -\gamma (\mathbf{X} \mathbf{X}^\top + \gamma \mathbf{I}_n)^{-1}$. We have $(\mathbf{H} - \mathbf{I}_n)^2 = \gamma^2 (\mathbf{X} \mathbf{X}^\top + \gamma \mathbf{I}_n)^{-2}$. The bias term becomes:

$$\begin{aligned} \mathbb{E} \text{tr} [\gamma^2 (\mathbf{X} \mathbf{X}^\top + \gamma \mathbf{I}_n)^{-2} \mathbf{XW}_0 \mathbf{W}_0^\top \mathbf{X}^\top] &= \gamma^2 \mathbb{E} \left[\text{tr} \left(\mathbf{W}_0^\top \mathbf{X}^\top (\mathbf{X} \mathbf{X}^\top + \gamma \mathbf{I}_n)^{-2} \mathbf{XW}_0 \right) \right] \\ &\leq \gamma^2 \mathbb{E} \left[\text{tr} \left(\mathbf{X}^\top (\mathbf{X} \mathbf{X}^\top + \gamma \mathbf{I}_n)^{-2} \mathbf{X} \right) \|\mathbf{W}_0\|_F^2 \right] \\ &\leq \gamma^2 M R^2 \mathbb{E} \left[\text{tr} \left(\mathbf{X}^\top (\mathbf{X} \mathbf{X}^\top + \gamma \mathbf{I}_n)^{-2} \mathbf{X} \right) \right] \end{aligned}$$

Using properties of semi-positive matrices and the identity:

$$\mathbb{E} \left[\text{tr} \left(\mathbf{X}^\top (\mathbf{X} \mathbf{X}^\top + \gamma \mathbf{I}_n)^{-2} \mathbf{X} \right) \right] \leq \frac{n M C_{\mathbf{X}}^2}{\gamma^2} \quad (51)$$

Then, the bias term is bounded by:

$$\text{Bias} \leq \gamma^2 M^2 R^2 \text{tr} \left(\mathbb{E} \left[\mathbf{X}^\top (\mathbf{X} \mathbf{X}^\top + \gamma \mathbf{I}_n)^{-2} \mathbf{X} \right] \right) \leq n M^2 R^2 C_{\mathbf{X}}^2 \quad (52)$$

Variance term. Using the identity: $\mathbf{H} - \mathbf{I}_n = -\gamma (\mathbf{X} \mathbf{X}^\top + \gamma \mathbf{I}_n)^{-1}$, we have

$$\text{tr} \left[\mathbb{E} (\mathbf{H} - \mathbf{I}_n)^2 \right] \sigma^2 = \gamma^2 \sigma^2 \mathbb{E} \left[\text{tr} \left((\mathbf{X} \mathbf{X}^\top + \gamma \mathbf{I}_n)^{-2} \right) \right]. \quad (53)$$

For semi-positive matrix $\mathbf{X} \mathbf{X}^\top$, we have $\text{tr} \left(\mathbb{E} \left[(\mathbf{X} \mathbf{X}^\top + \gamma \mathbf{I}_n)^{-2} \right] \right) \leq \frac{n}{\gamma^2}$. Thus, the variance term is bounded by:

$$\text{Variance} \leq n \sigma^2. \quad (54)$$

Combining the bias and variance bounds, we will get the final bound. \square

Remark. The result obtained in Lemma 3.6 aligns with the works of [Hsu et al. \(2012\)](#) and [Mourtada & Rosasco \(2022\)](#). For clarity of exposition and to stay within the theoretical framework of [Peng et al. \(2024\)](#), we have rederived a rough bound.

Lemma 3.7 (Wainwright (2019), Theorem 6.1). Let $\mathbf{X} \in \mathbb{R}^{n \times d}$ be drawn according to the Σ -Gaussian ensemble. Then for all $\delta > 0$, the maximum singular value $\sigma_{\max}(\mathbf{X})$ satisfies the upper deviation inequality,

$$\mathbb{P} \left[\frac{\sigma_{\max}(\mathbf{X})}{\sqrt{n}} \geq \lambda_{\max}(\sqrt{\Sigma})(1 + \delta) + \sqrt{\frac{\text{tr}(\Sigma)}{n}} \right] \leq e^{-n\delta^2/2}. \quad (55)$$

Moreover, for $n \geq d$, the minimum singular value $\sigma_{\min}(\mathbf{X})$ satisfies the analogous lower deviation inequality,

$$\mathbb{P} \left[\frac{\sigma_{\min}(\mathbf{X})}{\sqrt{n}} \leq \lambda_{\min}(\sqrt{\Sigma})(1 - \delta) - \sqrt{\frac{\text{tr}(\Sigma)}{n}} \right] \leq e^{-n\delta^2/2}, \quad (56)$$

Algorithm 1 Our STSA for FCIL

Input: Datasets: $\{\mathcal{D}_{1:T,1:K}\}$, initial model: θ , initial random seed: SEED.

Initialization: server distributes the initial model and the initial random seed SEED to all clients. Each client initializes a random mapping layer R using SEED.

foreach each task $t = 1, \dots, T$ **do**

if $t = 1$ **then**

 └ Update θ in federated manner. Fix the feature extractor F .

foreach each client $i = 1, \dots, K$ **do**

if STSA-E **then**

 └ Extract Spatial Statistics $\mathbf{C}_{t,k}$ and $\mathbf{n}_{t,k}$;

else

 └ Extract Spatial Statistics $\{\mathbf{G}_{t,k}, \mathbf{C}_{t,k}\}$;

 Spatial Statistics Aggregation via Eq. 2;

 Temporal Statistics Aggregation via Eq. 4;

if STSA-E **then**

 └ Obtain $\hat{\mathbf{G}}_t$ via Eq. 9;

 └ Update classifier \mathbf{W}_t via Eq. 10;

else

 └ Update classifier \mathbf{W}_t via Eq. 8;

return $\theta_t = \{F, R, \mathbf{W}_t\}$

where $\lambda_{\max}(\cdot), \lambda_{\min}(\cdot)$ means the maximum and minimum eigenvalue respectively.

Remark. Lemma 3.7 demonstrates that the following statement holds, which is used in the proof of Theorem 3.3. With a probability of at least $1 - e^{-n\delta^2/2}$,

$$\lambda_{\min}(\mathbf{X}\mathbf{X}^\top) \geq n \left(\lambda_{\min}(\sqrt{\Sigma})(1 - \delta) - \sqrt{\frac{\text{tr}(\Sigma)}{n}} \right)^2 = O(n). \quad (57)$$

Lemma 3.8(Wainwright (2019), Exercise 6.1). Given two symmetric matrices \mathbf{A} and \mathbf{B} , we have

$$|\lambda_{\max}(\mathbf{A}) - \lambda_{\max}(\mathbf{B})| \leq \|\mathbf{A} - \mathbf{B}\|_2 \quad \text{and} \quad |\lambda_{\min}(\mathbf{A}) - \lambda_{\min}(\mathbf{B})| \leq \|\mathbf{A} - \mathbf{B}\|_2. \quad (58)$$

Remark. Lemma 3.8 demonstrates that the following statement, which is used in the proof of Theorem 3.3.

$$|\lambda_{\min}(\mathbf{A})| = |\lambda_{\min}(\mathbf{B}) - (\lambda_{\min}(\mathbf{B}) - \lambda_{\min}(\mathbf{A}))| \geq |\lambda_{\min}(\mathbf{B})| - |\lambda_{\min}(\mathbf{B}) - \lambda_{\min}(\mathbf{A})| \geq |\lambda_{\min}(\mathbf{B})| - \|\mathbf{A} - \mathbf{B}\|_2. \quad (59)$$

D. Pseudo-Code

We provide the the summary of the entire STSA procedure with pseudocode in Algorithm 1.

E. Experimental Details

E.1. Evaluation Metrics

In this work, we employ three widely-used metrics in CIL: average incremental accuracy (A_{avg}), final average accuracy (A_T), and average forgetting (F_T). A_{avg} denotes the average performance across all incremental stages, A_T is the accuracy averaged over all T tasks after completing task \mathcal{T}_T , and F_T represents the average performance decline on previous tasks over all T tasks. Let $A_{t,\tau}$ represent the classification accuracy on the τ -th task after training on the t -th task. After training

on the t -th task, we calculate the evaluation metrics as follows:

$$A_{\text{avg}} = \sum_{t=1}^T \frac{1}{t} \sum_{\tau=1}^t A_{t,\tau}, \quad (60)$$

$$A_T = \frac{1}{T} \sum_{\tau=1}^T A_{T,\tau}, \quad (61)$$

$$F_T = \frac{1}{T-1} \sum_{\tau=1}^{T-1} \max_{\tau' \in \{1, \dots, T-1\}} A_{\tau', \tau} - A_{T,\tau}. \quad (62)$$

E.2. Client Training Details

For the training-from-scratch setting, we follow the configurations from Tran et al. (2024), using ResNet18 (He et al., 2016) as the backbone. Each client is trained using a batch size of 128 for 100 communication rounds, with 2 local training epochs per round. For CIFAR100 (Krizhevsky et al., 2009), we employ the SGD optimizer with a learning rate of 0.04, a momentum of 0.9, and a weight decay of 5×10^{-4} . For Tiny-ImageNet (Le & Yang, 2015), we use a learning rate of 0.1, a weight decay of 2×10^{-4} , and a multi-step learning rate scheduler that reduces the learning rate by a factor of 10 at the 50th and 75th communication rounds.

When training from pre-trained model, we incorporate an adapter into each layer of pre-trained ViT via residual connections to facilitate parameter-efficient tuning (Zhou et al., 2024a). Specifically, an adapter typically consists of a downsampled MLP layer $W_{\text{down}} \in \mathbb{R}^{d \times r}$, a non-linear activation function ReLU, and an upsampled MLP layer $W_{\text{up}} \in \mathbb{R}^{d \times r}$. We formulate the output of the MLP when using the adapter as follows:

$$\mathbf{x}_o = \text{MLP}(\mathbf{x}_i) + s * \text{ReLU}(\mathbf{x}_i W_{\text{down}}) W_{\text{up}}, \quad (63)$$

where \mathbf{x}_i represent the input, \mathbf{x}_o denote the output, and s be the scale factor. By default, the scale factor s is set to 0.1, and the projection dimension r for the adapter is fixed at 64. For clients' local training, we use a learning rate of 0.2 and a weight decay of 5×10^{-4} . The model is trained with a batch size of 128 for 2 local epochs. It runs for 10 communication rounds on CIFAR100 (Krizhevsky et al., 2009) and 20 communication rounds on ImageNet-R (Hendrycks et al., 2021).

E.3. Additional Results

Full results of ablations study are shown in Figure 8 and Figure 9.

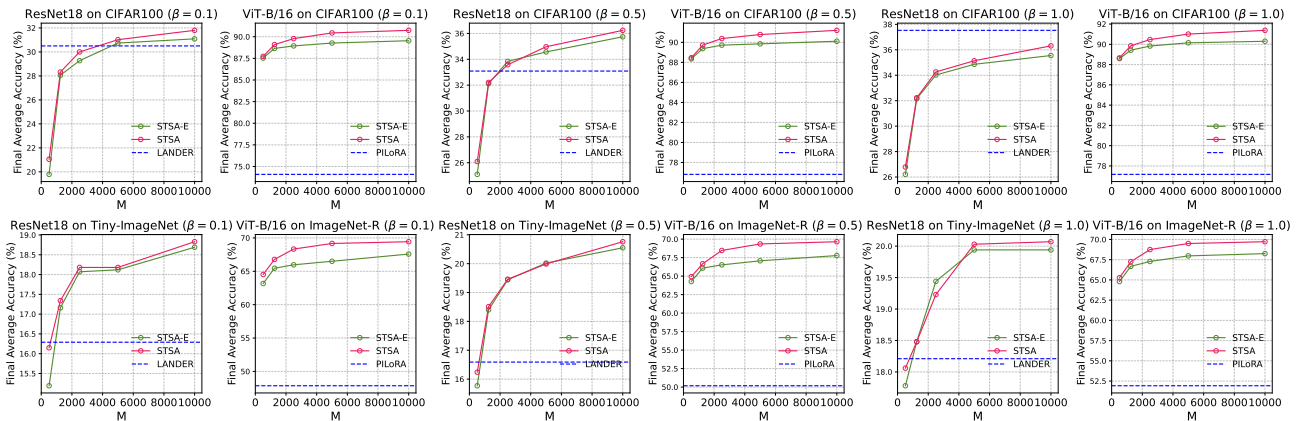


Figure 8. Ablation study on the dimension of random features (M). For ResNet18, M varies across $\{512, 1250, 2500, 5000, 10000\}$, while for ViT, it varies across $\{768, 1250, 2500, 5000, 10000\}$. $M = 512$ corresponds to the raw feature dimension of ResNet18, and $M = 768$ corresponds to the raw feature dimension of ViT, indicating no random mapping is applied. The performance of the top-performing baselines (LANDER and PILoRA) is marked with a blue horizontal line in the figure.

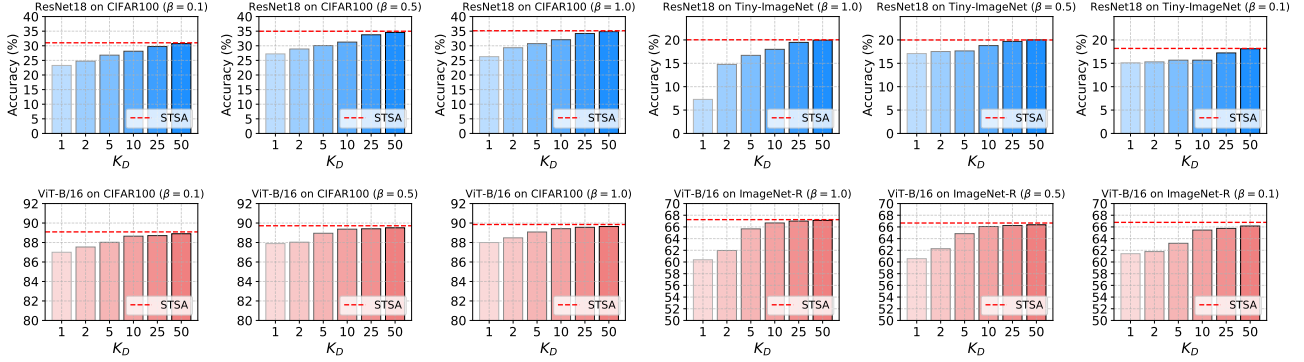


Figure 9. Ablation study on the number of dummy clients (K_D). We test K_D values in $\{1, 2, 5, 10, 25, 50\}$. When $K_D = 1$, no dummy clients are used. The performance of STSA is shown as a red horizontal line in the figure. Dummy clients are introduced to address scenarios with insufficient client numbers (e.g., cross-soil settings). When the number of clients is already large (e.g., cross-device settings), dummy clients are not needed.

F. Privacy Discussion

In our STSA, uploading Spatial Statistics may pose privacy concerns. Specifically, STSA uploads $G_{t,k}$ and $C_{t,k}$, while STSA-E uploads $C_{t,k}$ and $n_{t,k}$ (assuming no dummy clients are used for simplicity). Feature statistics $G_{t,k}$ and $C_{t,k}$ are the aggregation of feature statistics from all local data samples. In real-world scenarios, each client k typically has many data samples across various classes, making it difficult to reconstruct specific samples from the uploaded feature statistics. To support this, we conduct feature inversion experiments (Ulyanov et al., 2018; Luo et al., 2021) to validate this claim. Label frequency $n_{t,k}$ has been widely used in numerous FL methods (Luo et al., 2021; Zhang et al., 2022; Gong et al., 2021; Zhu et al., 2021; Wang et al., 2024; Heinbaugh et al., 2023), and label frequency presents fewer privacy risks compared to data samples.

F.1. Feature Inversion Details

Here, we consider the scenario where the target client k has only a few samples (3 samples) from the same class (“apple” in CIFAR100), and the attacker utilizes the uploaded Spatial Statistics to attempt reconstruction of a specific training data sample using feature inversion technology, as shown in Ulyanov et al. (2018); Luo et al. (2021). In this case, the uploaded Spatial Statistics is a mixture of features from a few samples (3 samples) within the same class, making it less mixed and thus more advantageous for the attacker. In addition to using the uploaded Spatial Statistics for feature inversion, we also provide experimental results for inversion using raw representations, where each raw feature corresponds to a single input sample. Table 6 presents the quantitative similarity metrics between the ground truth and the reconstructed results. Higher PSNR and SSIM values and lower LPIPS values indicate greater similarity to the ground truth, demonstrating better attack performance. For our STSA, we compute similarity measures between the inversion result and each real sample, then average them to derive the final results. Figure 10 presents the visualization results of feature inversion. When using the raw feature of a specific data sample, the inversion produces clear visual outputs with higher quantitative similarity metrics. In contrast, using our uploaded Spatial Statistics for feature inversion leads to significantly worse metrics. The visual results consist of irregular color patches, making it hard to discern information related to the original data samples.

F.2. Compatibility with Privacy-Preserving Techniques

Secure aggregation is especially suitable for our STSA, since the server only needs the aggregated Spatial Statistics, not the individual value from each client. Additionally, we can add random noise to the uploaded Spatial Statistics to enhance the privacy-preserving capabilities of our method (Tan et al., 2022; Zhang et al., 2024b).

Table 6. Quantitative similarity measures of inversion results. For our STSA, we compute similarity measures between the inversion result and 3 real samples, then average them to obtain the final results.

Reconstruction Source	Similarity Measure		
	$PSNR \downarrow$	$SSIM \downarrow$	$LPIPS \uparrow$
Raw Feature 1	18.43	0.68	0.26
Raw Feature 2	22.15	0.77	0.14
Raw Feature 3	19.84	0.79	0.19
STSA-E	<u>11.43</u>	<u>0.34</u>	<u>0.79</u>
STSA	11.18	0.26	0.84

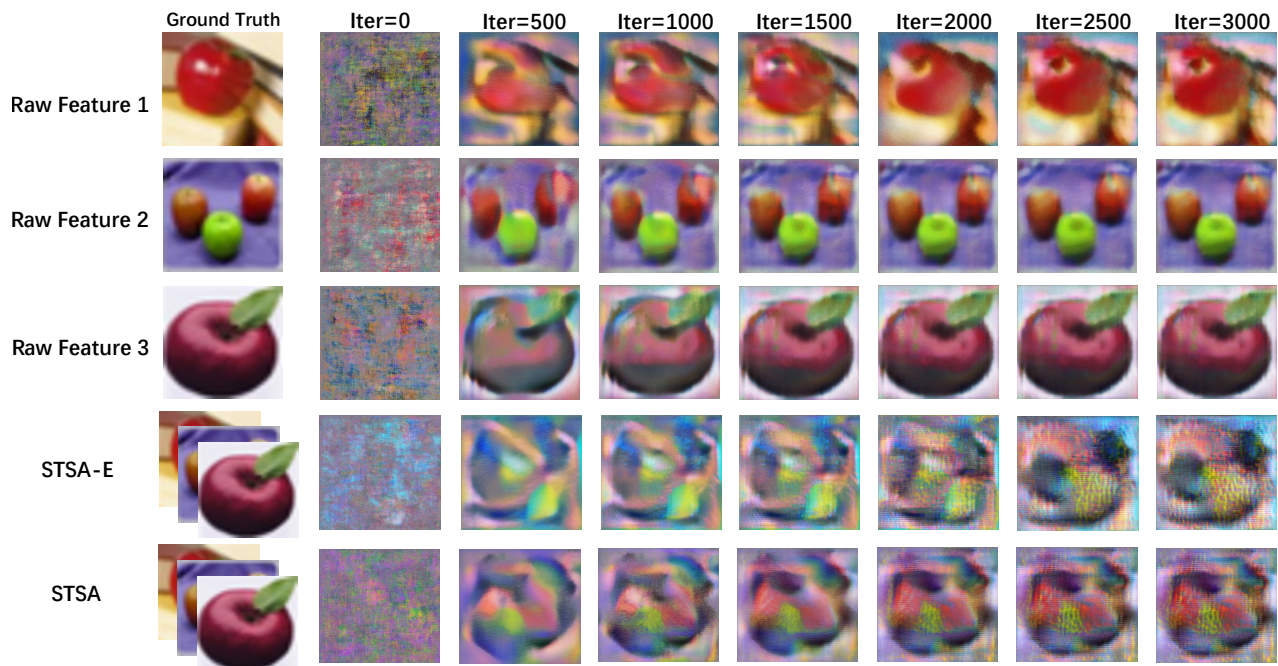


Figure 10. Results of feature inversion on CIFAR10. Assume a client has only three "apple" samples. An attacker tries to reconstruct a data sample from this client. When the attacker accesses the **Raw Features** of a specific sample, the reconstructed results are clear. However, using our uploaded statistics, the reconstruction quality significantly deteriorates.